

Numerical models for assessing the performance of heat pumps with maldistribution effects in plate heat exchanger evaporators

Heat pump cycle design, heat exchanger design, coupled cycle-heat exchangers off-design performance

by:

Roberta Mancini

PhD student

Section of Thermal Energy

Department of Mechanical Engineering
Technical University of Denmark (DTU)

robman@mek.dtu.dk

Documentation revised by:
Benjamin Zühdorf (DTU)

and approved by:
Brian Elmegaard (DTU)



Contents

1	Introduction	1
2	Numerical models	3
2.1	Plate heat exchanger model	3
2.1.1	PHE Geometry	3
2.1.2	Governing equations	5
2.1.3	Discretization approach	6
2.1.4	Numerical model	7
2.1.5	Iterative solution strategy	9
2.1.6	Choice of correlations	12
2.1.7	Solver for the design problem	17
2.2	Coupled HP-PHE off-design model	19
2.2.1	Coupled HP-PHE off-design model without maldistribution effects	19
2.2.2	Coupled HP-PHE off-design model with maldistribution effects .	21
3	Validation and verification	25
3.1	Flow distribution solver verification	25
3.2	Comparison with experimental data: evaporation data from DTU	27
3.3	Comparison with experimental data: condensation data from DTU	29
3.4	Solution sensitivity to model tolerances	30
3.5	Grid independence study	33
4	User guide	35
4.1	System requirements	35
4.2	Model structure	35
4.2.1	Model inputs	37
4.2.2	Model outputs	37
	Final remarks	39
	Bibliography	39

1 Introduction

This documentation provides background, detailed information and user guide to the numerical models presented and applied in [1]. The models were used in order to estimate the effect of end plates and the impact of liquid/vapour maldistribution in plate heat exchanger (PHE) evaporators on the thermodynamic and economic performance of heat pumps (HPs). The flow of the simulation procedure is presented in Fig. 1.1. The flow-chart shows how the different models are integrated in the overall procedure. Each rectangle represents a numerical model, while each parallelepiped represents input/output of the models. The rounded bold rectangles represent instead the main outputs.

The user is also able to use each model for "stand-alone" calculations for both design and performance analysis of cycle only, PHE only or coupled HP-PHE simulations. Both pure fluids and binary mixtures of variable composition can be chosen as working fluids. The capabilities of the overall procedure are (following the structure of the flowchart):

- **Heat pump design model.** After defining the boundary conditions of the cycle and the working fluid, the design of the heat pump is carried out. The reader is referred to [2] for a comprehensive description of the modelling strategy adopted for cycle calculations.
- **Evaporator and condenser design models.** A design model aims at estimating the required heat transfer area to meet a defined thermal load. The inputs are therefore given by the mass flow rate and inlet thermodynamics of both working fluids, together with the design heat flow rate. The solver used for the design problem is described in details in chapter 2.1.7. In the simulation framework, two different models can be found for evaporator and condenser components of the heat pump. The models are based on a solver for heat transfer and fluid flow. Therefore, pressure drops of both fluids and real outlet thermodynamics are obtained as additional outputs.
- **Heat pump off-design model.** The off-design calculations are carried out by an overall simulation framework (yellow box in Fig.1.1), including a solver of heat transfer and fluid flow of both evaporator and condenser, as well the calculations of compressor operation in off-design. Chapter 2.2 includes a comprehensive description of the models.

Chapter 1. Introduction

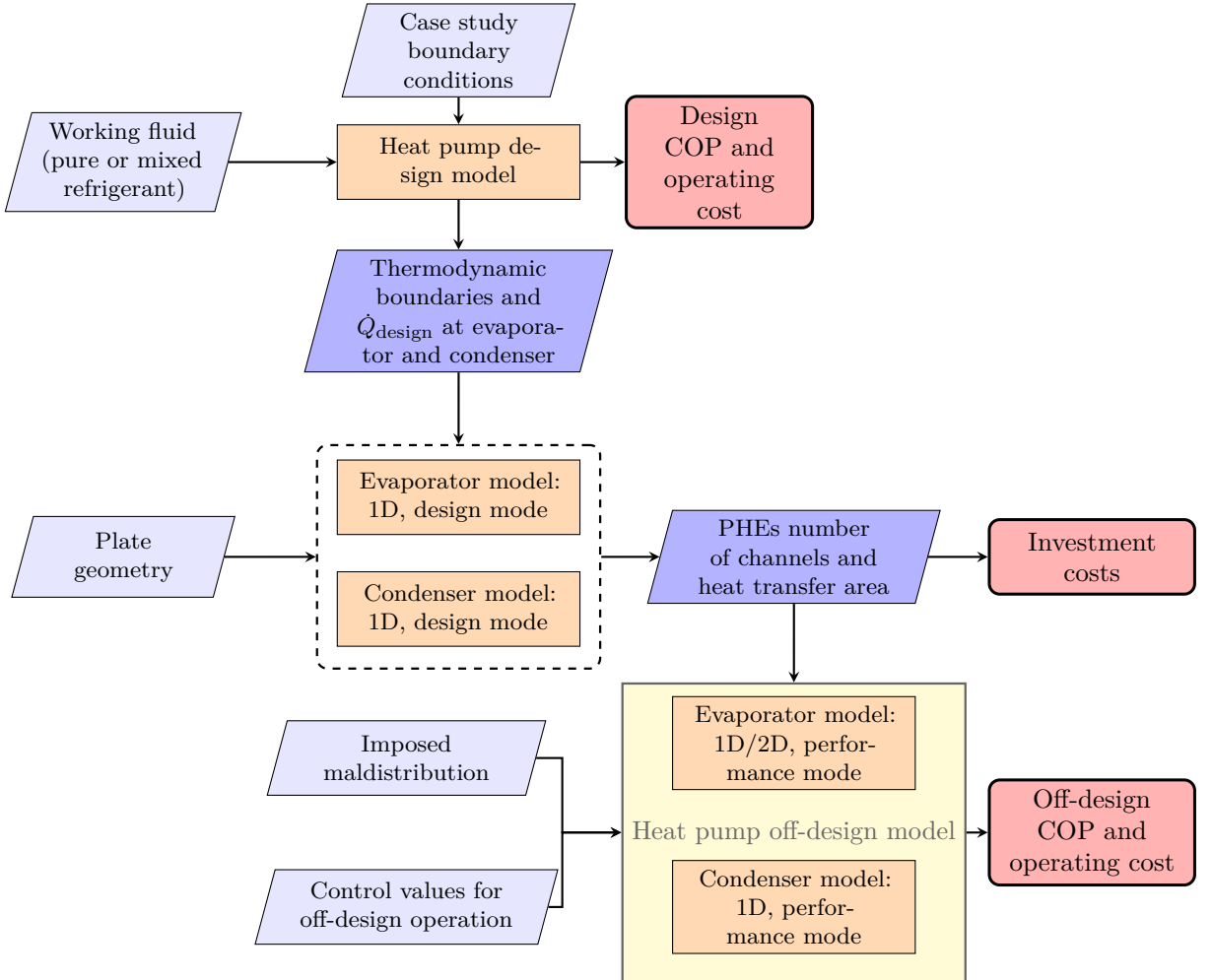


Figure 1.1: Work flow of the overall procedure. Rectangles represent a numerical model; parallelepipeds represent input/output; rounded bold rectangles represent main output. Adapted from [1]

This documentation is structured as follow:

- Chapter 2 describes in details the heat exchanger (HEX) and coupled PHE - heat pumps models. The different solvers implemented to solve the design and performance problems are also presented.
- Chapter 3 shows the results of the validation of the internal solver for heat transfer and fluid flow against available experimental data. Moreover, the verification of the flow distribution solver for single-phase flow against another study is also shown.
- Chapter 4 briefly indicates the system requirements to run the models and gives an introductory guide in order to understand the structure and functioning of the models.

2 Numerical models

This chapter explains the mathematical formulation of the PHE models. Moreover, all the solvers implemented in order to solve the design and performance problems are presented. First the PHE models, discretization and governing equations are presented in section 2.1. This section additionally reports the implementation of the solver for heat transfer and fluid flow and all the correlations implemented in the simulation framework (2.1.6). The solver for heat transfer and fluid flow is the base for the implementation of the PHE design solver, presented in subsection 2.1.7. Finally, two coupled heat pump - PHE off-design models are presented in section. 2.2

2.1 Plate heat exchanger model

In this section, the formulation of the PHE model that was implemented in the framework is presented. Depending on the type of analysis carried out, the different problems of design, rating and performance were addressed and different solvers were coupled with the model. However, the mathematical formulation of the PHE model was analogous in all the cases, i.e. aiming at solving mass, momentum and energy conservation equations in the PHE. In the following subsection, a detailed description of the PHE geometry, the governing equations describing the fluid flow and heat transfer mechanism, as well as the adopted discretization method and the numerical implementation, is presented. MATLAB 2017b [3] was used as programming framework.

2.1.1 PHE Geometry

The geometry of a chevron-PHE is determined by plate size and count, and corrugation specific parameters. An illustrative example is depicted in Fig. 2.1, while Table 2.1 reports the list of the parameters. The plate size is defined by width W and length. The port-to-port length L_p characterizes the fluid flow length, affecting the pressure drop. The heat transfer length L_{ht} is the effective plate length determining the heat transfer area. The number of plates defines the number of channels for fluid flow N_{ch} , and thus the total heat transfer area. The plate thickness t determines the trade-off between mechanical integrity of the component and wall thermal conductive resistance. The plates are most commonly manufactured in stainless steel, with a thermal conductivity k_w equal to 16.2 W/(mK). Last, the port diameter D_p determines the inlet and outlet

Chapter 2. Numerical models

pressure drop.

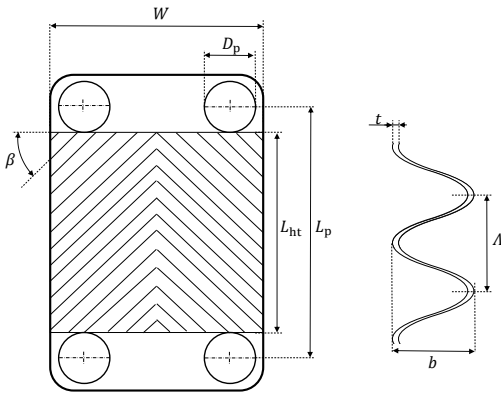
The corrugation geometry is characterized by corrugation pitch Λ , plate spacing (or corrugation height) b , and chevron angle β . Literature reports different definitions of β as the angle with the vertical or horizontal axis. In this work, the chevron angle β is estimated with respect to the horizontal axis (see Fig.2.1), while the complement $\theta = 90^\circ - \beta$ indicates the inclination angle, e.g. the angle with the vertical axis. A high β (equal to a low θ) corresponds to designs resulting in high heat transfer coefficients and high pressure drop, while a low β entails low pressure drop and lower heat transfer coefficient. The corrugation geometry is thus a key-set of parameters determining both heat transfer and pressure drop in the inter-plate passages.

The calculation of the channel hydraulic diameter, free-flow area, and effective heat transfer area was carried out by using the correlations proposed by Martin [4]. The hydraulic diameter D_h was estimated by Eq.(2.1).

$$D_h = \frac{2b}{\Phi} \quad (2.1)$$

Here, Φ indicates the enlargement factor, i.e. the ratio between effective and flat plate area. Φ is determined as a function of corrugation pitch and plate spacing, estimated by Eq.(2.2).

$$\Phi = \frac{1}{6} \left(1 + \sqrt{1 + \left(\frac{\pi b}{\Lambda} \right)^2} + \sqrt{1 + \frac{1}{2} \left(\frac{\pi b}{\Lambda} \right)^2} \right) \quad (2.2)$$



Parameter	Description
W	Plate width
L_p	Port-to-port length
L_{ht}	Heat transfer length
N_{ch}	Number of channels
b	Corrugation height
Λ	Corrugation pitch
β	Chevron angle
θ	Inclination angle
t	Plate thickness
k_w	Thermal conductivity

Figure 2.1: Chevron PHE geometry **Table 2.1: Geometrical parameters**

The free-flow area of each fluid was computed as:

$$A_0 = b \cdot N_{ch} \cdot W \quad (2.3)$$

where N_{ch} indicates the number of channels in which the considered fluid is flowing. The total heat transfer area is finally determined by Eq.(2.4). The number of channels in PHE is typically an odd number, with the secondary fluid flowing in the outer channels.

2.1. Plate heat exchanger model

Due to the assumption of adiabatic end-plates, the number of channels in Eq.(2.4) must be referred to the value of the working fluid with the lowest number of channels.

$$A_{\text{ht}} = 2 \cdot \Phi \cdot (W \cdot L_{\text{ht}}) \cdot N_{\text{ch}} \quad (2.4)$$

2.1.2 Governing equations

The governing equations are given by mass, momentum and energy conservation equations. The following assumptions were considered:

- (i) steady state conditions;
- (ii) adiabatic end plates, i.e. no heat loss to the environment;
- (iii) no longitudinal conduction through the plates;
- (iv) liquid and vapour phases flowing at different velocities according to an estimated slip ratio;
- (v) no pressure drop in the PHE manifolds;
- (vi) Newtonian working fluids.

Given the PHE geometry, with constant free-flow area A_0 for each fluid path, the steady-state mass conservation equation results in:

$$G = \text{const.} \quad (2.5)$$

where G is the mass flux of the fluid flowing in the channel. The momentum equation was given by Eq.(2.6), where the three terms represent the frictional (fr), gravity (gr) and acceleration (acc) contributions to the total pressure drop, and f indicates the Fanning friction factor.

$$\frac{dp}{dz} = -2f \frac{G^2}{\rho D_h} - \frac{d(\rho g z)}{dz} - G^2 \frac{1}{dz} \left(\frac{1}{\rho} \right) = \left(\frac{dp}{dz} \right)_{\text{fr}} + \left(\frac{dp}{dz} \right)_{\text{gr}} + \left(\frac{dp}{dz} \right)_{\text{acc}} \quad (2.6)$$

The energy conservation equation in steady state for both primary and secondary fluids was expressed by Eq.(2.7) for single-phase flow and by Eq.(2.8) for two-phase flow. In Eq.(2.8), the kinetic contribution to energy balance was neglected.

$$\dot{m} c_p \frac{dT}{dz} = \sum_{m=1}^{n_w} P^m U^m (T_w^m - T) \quad (2.7)$$

$$\dot{m} \frac{di}{dz} = \sum_{m=1}^{n_w} P^m U^m (T_w^m - T) \quad (2.8)$$

Here, i indicates the enthalpy, P^m represents the heat transfer perimeter, z is the direction of the fluid flow, and n_w is the total number of walls that are in contact with the fluid.

Chapter 2. Numerical models

The overall heat transfer coefficient U^m is determined by the convective heat transfer coefficient of the fluid and by the conductive resistance of half thickness of wall, and calculated by:

$$U^m = \left(\frac{1}{h^m} + \frac{t/2}{k_w} \right)^{-1} \quad (2.9)$$

2.1.3 Discretization approach

Two different approaches were implemented, applying a one-dimensional (1D) and a two-dimensional (2D) discretization, respectively. The 2D discretization was applied to the evaporator performance model, since it can account for the flow distribution in the different channels. The 1D discretization was applied to both evaporator and condenser design and performance models. The difference between the results of the 1D performance model of the evaporator and the 2D model with uniform vapour quality distribution at the inlet allows estimating the effect of end plates, since the flow is assumed to distribute perfectly even among the different channels in the 1D case. The different discretization approaches are shown for the example of the evaporator in Fig.2.2, where hs indicates the heat source (or secondary fluid) and ref the refrigerant cells. The 2D discretization, represented in Fig.2.2 (b), divides the PHE into n slices along the flow direction. The grid is further discretized by dividing each slice by the total number of channels. One CV is therefore constituted by a refrigerant or a secondary fluid cell and half thickness of the plate. Two adjacent refrigerant and secondary fluid CVs share thus a face at the midpoint of the wall. This kind of discretization allows considering different mass flow rates (shown by $\dot{m}_{ref/hs}(j)$) at each channel j of the PHE. Fig.2.2 (a) represents the 1D discretization, solely applied along the flow direction. In each slice two different CV are

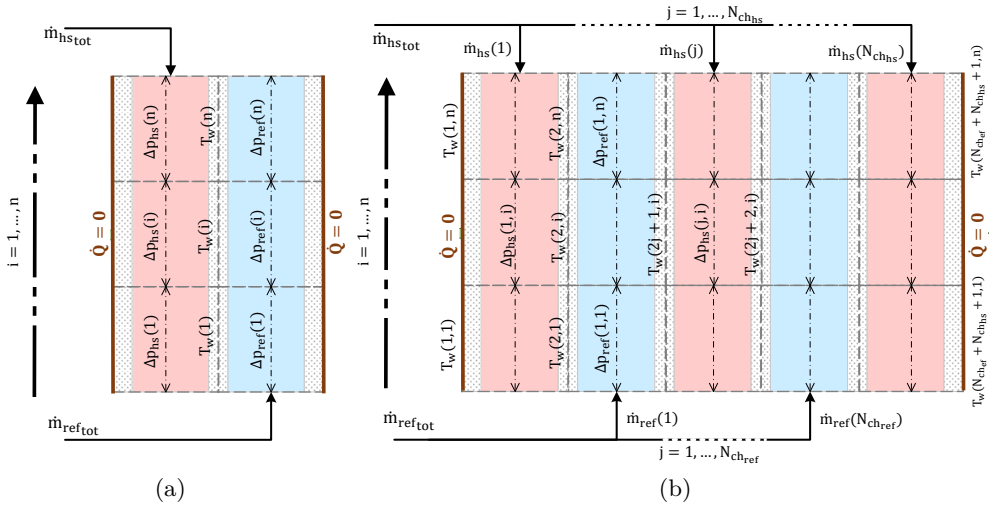


Figure 2.2: PHE model discretization approaches:(a) 1D ; (b) 2D

2.1. Plate heat exchanger model

considered to describe the refrigerant and the secondary fluid flows. One face of two adjacent CVs is shared also in this case, by placing each CV boundary at the midpoint of the plate wall.

Note that, in both cases, a centered approach was chosen for wall discretization. Two adjacent fluid cells shared a boundary at the midpoint of the plate thickness, and the wall temperature was estimated at the center point between inlet and outlet of both fluid paths [5].

2.1.4 Numerical model

The momentum (Eq.(2.6)) and energy (Eq.(2.7) and Eq.(2.8)) conservation equations were integrated in each cell by a finite volume method, since local conservation ensures global conservation over the entire fluid domain. As shown in Fig.2.2 the total mass flow rate of one fluid was considered to flow simultaneously in one equivalent channel with area equivalent to the sum of all channels in the 1D case, while each channel is considered separately in the 2D case.

Fig. 2.3 shows the details of the discretization schemes in both 1D and 2D. The black squares (for pressure p and enthalpy i) indicate the values evaluated at the nodes, i.e. at the inlet/outlet of each cell. The orange square indicates the value at the center point, which was evaluated by a central differencing scheme assuming a linear variation between inlet and outlet. The wall temperature (blue square) in each CV was evaluated at the midpoint between inlet and outlet of one fluid cell.

For a specific CV (j,i) the integration of the momentum equation led to the formulation in Eq.(2.10). In this notation, the row index j identifies the channel, while the column index identifies the CV along the flow direction. The 1D formulation is analogous (with no index j).

$$p_{\text{nodes}}^{(j,i+1)} = p_{\text{nodes}}^{(j,i)} - \Delta p_{\text{fr}}^{(j,i)} - \Delta p_{\text{gr}}^{(j,i)} - \Delta p_{\text{acc}}^{(j,i)} \quad (2.10)$$

Note that the pressure drop $\Delta p^{(j,i)}$ is evaluated by using the fluid properties at the center of the CV, and then applied to estimate the value of the pressure at the outlet of the CV $p_{\text{nodes}}^{(j,i+1)}$. A more detailed explanation of the computation of frictional, gravity and acceleration contributions to pressure drop is presented in section ??.

The energy conservation equation for single-phase flow was solved by assuming a linear variation of the fluid temperature in the CV. In the 2D discretization scheme, each channel has a right (R) and left (L) wall exchanging thermal energy with the fluid cell, thus the integral formulation of Eq.(2.7) for the CV (j,i) leads to:

$$\int_{j,i}^{j,i+1} dT = \int_{z^{j,i}}^{z^{j,i+1}} \left[\frac{P^{(j,i)} U^{(j,i)}}{\dot{m}^{(j)} c_p} (T_{w,R}^{(j,i)} - T) + \frac{P^{(j,i)} U^{(j,i)}}{\dot{m}^{(j)} c_p} (T_{w,L}^{(j,i)} - T) \right] dz \quad (2.11)$$

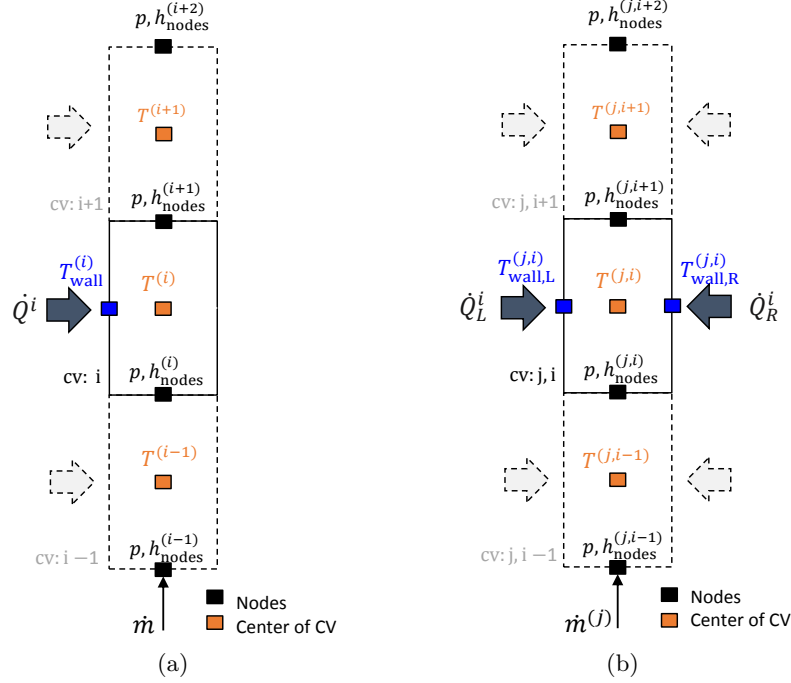


Figure 2.3: Detailed discretization schemes: (a) 1D, (b) 2D

From the integration of Eq.(2.11), it holds:

$$T_{\text{nodes}}^{(j,i+1)} = \frac{\chi(T_{w,L}^{(j,i)} + T_{w,R}^{(j,i)}) + (1 - \chi)T_{\text{nodes}}^{(j,i)}}{1 + \chi} \quad (2.12)$$

with χ equal to:

$$\chi = \frac{\Delta A_{\text{ht}}^{(j,i)} U^{(j,i)}}{\dot{m}^{(j)} c_p} \quad (2.13)$$

The advantage of using the formulation of Eq.(2.12), is that the temperature at the outlet of the cell can be computed by solely using the inlet value and the wall temperature of the cell. In two-phase flows, the energy conservation must be expressed in terms of enthalpy i , and the integration of Eq.(2.8) leads to the formulation:

$$i_{\text{nodes}}^{(j,i+1)} = i_{\text{nodes}}^{(j,i)} + \frac{\Delta A_{\text{ht}}^{(j,i)} U^{(j,i)}}{\dot{m}^{(j)}} (T_{w,R}^{(j,i)} - T^{(j,i)}) + \frac{\Delta A_{\text{ht}}^{(j,i)} U^{(j,i)}}{\dot{m}^{(j)}} (T_{w,L}^{(j,i)} - T^{(j,i)}) \quad (2.14)$$

Here, since the temperature of the fluid at the center of the fluid cell $T^{(j,i)}$ is not known, the calculation was carried out as suggested by Corberán [6], e.g. to assume

2.1. Plate heat exchanger model

the temperature equal to the value at the inlet node plus a variation equal to the previous iteration variation. Moreover, in order to compute the different contributions to pressure drop in Eq.(2.10) and the heat transfer coefficients U in Eq.(2.12) and (2.14), fluid thermo-physical properties are evaluated at the center of the cell. Assuming a linear variation of the fluid thermo-physical properties, the same approach used for the temperature was adopted, and translated into:

$$\Psi_k^{(j,i)} = \Psi_{\text{nodes},k}^{(j,i)} + \frac{\Psi_{\text{nodes},k-1}^{(j,i+1)} - \Psi_{\text{nodes},k-1}^{(j,i)}}{2} \quad (2.15)$$

where Ψ represents a general property or temperature, k indicates the iteration number and (j,i) the CV taken into account.

In the 1D case, the energy conservation equations were slightly modified for both single-phase and two-phase flow, since each fluid CV is in contact with one wall only ($n_w = 1$ in Eq.(2.7) and (2.8)). For single-phase flow, the formulation was [5]:

$$T_{\text{nodes}}^{(i+1)} = \frac{\chi T_w^{(i)} + (1 - \chi/2) T_{\text{nodes}}^{(i)}}{1 + \chi/2} \quad (2.16)$$

with χ expressed by Eq.(2.13). For two-phase flow, instead, it was obtained:

$$i_{\text{nodes}}^{(i+1)} = i_{\text{nodes}}^{(i)} + \frac{\Delta A_{\text{ht}}^{(i)} U^{(i)}}{\dot{m}} (T_w^{(i)} - T^{(i)}) \quad (2.17)$$

2.1.5 Iterative solution strategy

The solution of the energy and momentum equations for the CVs of the domain requires the values of the mass flow rates and inlet thermodynamics of both fluids, which are imposed as boundary conditions at the inlet of the first nodes. In the 2D discretization scheme, the inlet mass flow rate in each channel is required for solving energy and momentum equations in all the cells of the considered channel. However the solution of the energy and momentum conservation equations requires the values of the wall temperature. Therefore, the overall solution strategy was implemented as an iterative procedure, and the solver was based on the SEWTLE (Semi-Explicit Wall Temperature Linked Equations) approach, presented in [5, 6]. Moreover, the alternate iteration approach suggested in [7] was implemented to accelerate the model convergence.

The flow-chart of the successive substitution solver, iterating on wall temperature and refrigerant and secondary fluid pressure drops, is shown in Fig.2.4. The inputs to the solver were given by the working fluid and the fully defined PHE geometry, together with the inlet thermodynamic state and mass flow rate of both fluids. The inlet state was used as boundary condition for the solution. An initial guess of the distribution of wall temperature and pressure drop was also provided to the solver. The guessed distribution for the wall temperature was given by a linear temperature variation between inlet refrigerant and secondary fluid temperatures, in order to avoid temperature crossing. Pressure drops were preliminarily calculated considering the fluid properties at the inlet

Chapter 2. Numerical models

conditions and distributed uniformly in each CV.

At each iteration k the temperature and the fluid thermo-physical properties were evaluated at the center of each cell. In the first iteration, the properties were estimated by considering the inlet conditions of the fluid entering the CV, which were known from the outlet of the previous cell. From the second iteration the values were estimated as suggested by Corberán et al. [5], and previously illustrated by Eq.(2.15). The refrigerant and secondary fluid heat transfer coefficients were evaluated by using the properties at the center of the CV, by means of appropriate experimental correlations. The thermodynamic state of both fluids at the outlet of the CV were subsequently estimated by integrating the momentum and energy balance equations locally. After solving energy and momentum conservation equations in all the refrigerant and secondary fluid cells, an energy balance over two adjacent refrigerant and secondary fluid cells was applied to compute an updated value of the wall temperature.

The balance led to the formulation of Eq.(2.18), where the heat transfer area was simplified being equal for both fluids.

$$T_{\text{wall}} = \frac{U_{\text{ref}} T_{\text{ref}} + U_{\text{sf}} T_{\text{sf}}}{U_{\text{ref}} + U_{\text{sf}}} \quad (2.18)$$

Here the subscript *ref* indicates the refrigerant and *sf* the secondary fluid, namely the heat source and heat sink sink for the evaporator and condenser, respectively. Using the wall temperature as iteration variable has the advantage of avoiding the convergence to unfeasible solutions, for example temperature crossing between fluids, compared to using the heat flux [7]. This method is also completely explicit with respect to the wall temperature, which is updated by Eq.(2.18) [6] as a function of the fluids temperature profiles and heat transfer coefficients.

The residuals between two subsequent iterations were estimated and the error was calculated as the L²-norm of the higher relative residuals between wall temperature, refrigerant and secondary fluid pressure drops. If the error was lower than the selected tolerance, the solution was given in terms of total heat flow rate, outlet thermodynamic states of the two fluids, as well as wall and fluid temperature and pressure distribution. If the error was higher than the tolerance, the solver updated the iteration variables and made an additional iteration. The solver in 2D needs as input the mass flow rate distribution of both fluids in the different channels. Therefore, the pressure drop across each channel was estimated as output of the model and it was not trivial that all the channels resulted in the same outlet pressure. The governing equations for the flow distribution were solved separately in the flow distribution solver, which will be presented in section 2.2.2.

2.1. Plate heat exchanger model

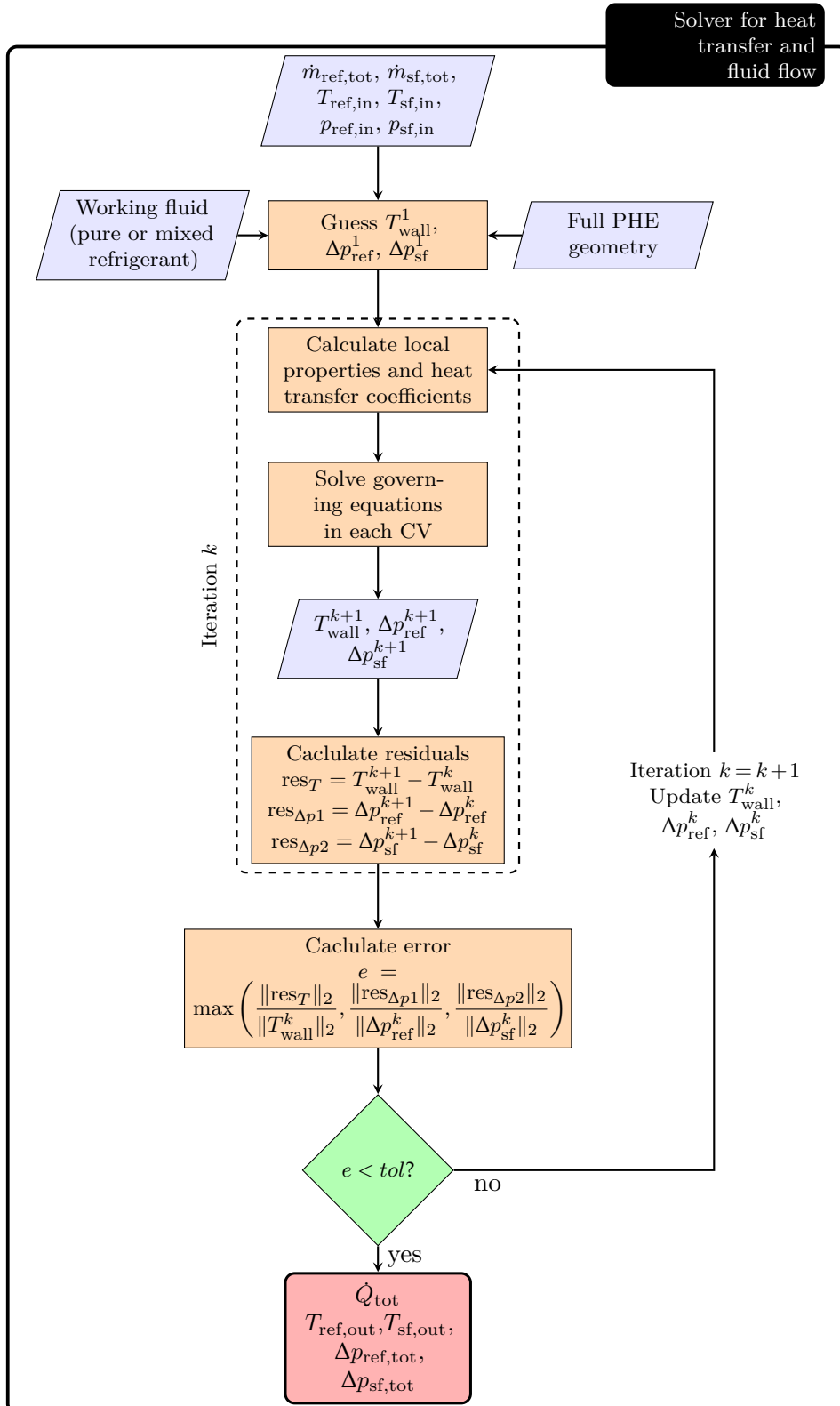


Figure 2.4: Work flow of the solver for heat transfer and fluid flow

2.1.6 Choice of correlations

Experimental correlations and theoretical models are implemented in order to estimate the heat transfer coefficients, the frictional pressure drops and the void fraction. It is out of the scope of this documentation to provide recommendation on the type of correlation to use in the models. It is up to the user to use an experimental correlation suitable for the working fluid, operating conditions and plate geometry. Since the correlations are implemented as functions of the different routines, the user is also able to implement additional models to the framework.

Heat transfer coefficients

Table 2.2 reports a list of correlation implemented and available for the estimation of the heat transfer coefficients in both two-phase flow and single-phase flow. The correlations were developed for pure fluids, thereby they can be directly used if a pure refrigerant is chosen as working fluid.

Different correction methods must be on the other hand used if a zeotropic mixture is chosen as working fluid. The corrections methods implemented in the simulation framework are reported in Table 2.3. The correction methods for nucleate boiling take into account the sole degradation of the nucleate boiling contribution to heat transfer. Correction methods for mixture evaporation take instead into account both nucleate boiling and convective boiling degradation. The user can also choose to directly apply a mixture specific correlation, reported as *mixtures specific correlations* in Table 2.3, which were however not developed for PHE geometry. If ammonia/water is chosen as working fluid, Taboas et al. [8] can be applied for flow boiling heat transfer coefficients.

The correction methods implemented for evaporation and condensation are briefly explained here, so that the user is able to understand their application. The Silver [9] and Bell-Ghaly [10] method was originally developed for mixture condensation and the extended to evaporation by Sardesai et al. [11].

Sardesai et al. [11] derived the formulation expressed by Eq.(2.19) to compute the mixture two-phase heat transfer coefficient during evaporation.

$$h_{\text{TP,evap}} = \frac{1 + h_{\text{NB-mix}}/h_C}{1/h_C + \bar{z}/h_V} \quad (2.19)$$

Here, $h_{\text{NB-mix}}$ is the nucleate boiling contribution of the mixture, h_C is the convective two-phase contribution and h_V is the single-phase vapour heat transfer coefficient estimated for the vapour flowing alone in the channel. \bar{z} is a correction term taking into account the ratio of sensible over latent heat transfer, and it is evaluated by Eq.(2.20) [10].

$$\bar{z} = x \cdot \frac{dT}{dh} \cdot c_{p,V} \quad (2.20)$$

In the estimation of $h_{\text{NB-mix}}$, the mixture effects on degradation of nucleate boiling and loss of effective wall superheat is accounted for by applying a suitable correction factor, for which different correlations exist and can be chosen. The ones implemented in the simulation framework are reported in the first section of Table 2.3.

2.1. Plate heat exchanger model

The formulation originally developed by Silver [9] and Bell-Ghaly [10] for mixture condensation is instead reported in Eq.(2.21), where h_C is the condensation heat transfer coefficient as the mixture was an ideal pure fluid and h_V is the single-phase vapour heat transfer coefficient estimated for the vapour flowing alone in the channel. \bar{z} is evaluated by Eq. (2.20), similarly to the evaporation case. The correlations to estimate h_C and h_V can be chosen among the ones for pure fluids, reported in Table 2.2, for single-phase vapour, two-phase convective evaporation and condensation.

$$h_{\text{TP,cond}} = \left(\frac{1}{h_C} + \frac{\bar{z}}{h_V} \right)^{-1} \quad (2.21)$$

Table 2.2: Available correlations for heat transfer coefficients

Model	Year	Ref.	Comments
<i>Single-phase</i>			
Chisholm and Wanniarachchi	1991	[12]	
Wanniarachchi et al.	1995	[13]	
Martin	1996	[4]	
Muley and Manglik	1999	[14]	
<i>Flow boiling (convective boiling dominated)</i>			
Danilova et al.	1981	[15]	
Yan and Lin	1999	[16]	
Han et al.	2003	[17]	
Amalfi et al.	2016	[18]	
Zhang et al.	2017	[19]	
<i>Nucleate boiling</i>			
Stephan and Abselsalam	1980	[20]	(not specific for PHE geometry)
Cooper	1984	[21]	
Palm and Claesson	2006	[22]	
Gorenflo	2010	[23]	
Steiner	2010	[24]	
Huang et al.	2012	[25]	
<i>Flow boiling (superposition models)</i>			
Hsieh and Lin	2003	[26]	
Longo et al.	2015	[27]	
<i>Condensation</i>			
Yan and Lin	1999	[28]	
Thonon and Bontemps	2002	[29]	
Han et al.	2003	[30]	
Longo et al.	2015	[31]	
Zhang et al.	2019	[32]	

Table 2.3: Implemented corrections methods for mixtures and mixture specific correlations for flow boiling

Model	Year	Ref.	Comments
<i>Correction methods for mixture nucleate boiling contribution</i>			
Stephan and Korner	1969	[33]	
Jungnickel et al.	1980	[34]	
Schlunder	1983	[35]	
Thome and Shackir	1987	[36]	
Fujita and Tsutsui	1994	[37]	
Fujita and Tsutsui	1997	[38]	
Inoue et al.	1998	[39]	
<i>Correction methods for mixture evaporation</i>			
Sardesai et al.	1982	[11]	extension of Silver and Bell-Ghaly to evaporation
<i>Correction methods for mixture condensation</i>			
Silver and Bell-Ghaly	1947/1973	[9, 10]	
<i>Mixtures specific correlations</i>			
Gungor and Winterton	1986	[40]	(not specific for PHE geometry)
Gungor and Winterton	1987	[41]	(not specific for PHE geometry)
Jung et al.	1989	[42]	(not specific for PHE geometry)
Wettermann and Steiner	2000	[43]	(not specific for PHE geometry)
<i>Ammonia/water specific correlations</i>			
Taboas et al.	2012	[8]	

Pressure drops

The PHE model, in both 1D and 2D, is able to estimate the pressure drop of both refrigerant and secondary sides by summing the different contributions of static (gravity), momentum (acceleration) and frictional pressure drops. The frictional pressure drops can be estimated by means of different methods and correlations. Such methods estimate the pressure drops locally by evaluating the refrigerant/secondary fluid local values of temperature, pressure and thermo-physical properties.

Table 2.4 reports the methods implemented in the simulation framework. The single-phase pressure drops can be estimated by different correlations calculating a Fanning friction factor. Vakili-Farahani et al. [44] did a comprehensive literature review on different approaches to estimate two-phase frictional pressure drops, reporting three different methods: (i) estimating a two-phase Fanning friction factor, (ii) applying the Lockhart-Martinelli [45] method and (iii) establishing a relation between pressure drops and kinetic energy per unit volume.

The two-phase Fanning friction factor can be estimated for both evaporation and condensation by the different correlations reported in Table 2.4, and pressure drops are

2.1. Plate heat exchanger model

subsequently calculated by:

$$\Delta p_{\text{fr,tp}} = 2f_{\text{tp}} \frac{\Delta L G^2}{\rho_m D_h} \quad (2.22)$$

where G represents the mass flux, ΔL indicates the plate length associated to the CV, D_h is the hydraulic diameter and ρ_m is the momentum density, estimated by:

$$\rho_m = \left(\frac{x^2}{\rho_V \alpha} + \frac{(1-x)^2}{\rho_L (1-\alpha)} \right) \quad (2.23)$$

where x is the vapour quality, α is the void fraction (estimated by an appropriate correlation) and the subscripts L and V indicate the liquid and vapour phases, respectively. The Lockhart-Martinelli [45] was extensively used in literature to estimate the two-phase frictional pressure drops by relating them to the single-phase *liquid alone* and *vapour alone* pressure drops as follow:

$$X^2 = \frac{\Delta p_L}{\Delta p_V} \quad (2.24)$$

$$\Phi_L^2 = \frac{\Delta p_{\text{fr,tp}}}{\Delta p_L} \quad (2.25)$$

Here, X is the so-called Lockhart-Martinelli parameter and Φ_L^2 is the two-phase frictional multiplier. Moreover, *alone* refers to the flow as the liquid/vapour occupies the entire cross-section of the channel, thus the mass flux used to estimate Δp_V and Δp_L must be multiplied by x and $(1-x)$, respectively.

The Lockhart-Martinelli method was developed for evaporation by using two approaches, reported in Table 2.4: Palm and Claesson [22] suggested to employ the correlation suggested by Chisholm [46] and reported in Eq.(2.26), to evaluate the two-phase multiplier and assuming the Chisholm parameter C equal to 4.67, fitted from their experimental data on PHEs, together with employing Martin [4] to estimate the single-phase frictional pressure drops. Taboas et al. [8] proposed instead to employ a Chisholm parameter C equal to 3 and to use their in-house developed correlation to estimate the single-phase pressure drops.

$$\Phi_L^2 = 1 + \frac{C}{X} + \frac{1}{X^2} \quad (2.26)$$

The last method implemented for the evaporation pressure drops was to define a proportionality between the frictional pressure drops and the kinetic energy per unit volume, as suggested for PHEs by Longo and Gasparella [47]. By employing this method, the

Chapter 2. Numerical models

pressure drops are estimated as:

$$\Delta p_{\text{fr,tp}} = \xi \frac{G^2}{2\rho_m} \quad (2.27)$$

where ξ is defined by the correlation.

For the condensation case, only correlations estimating the two-phase Fanning friction factor were included in the simulation framework. Note that, similarly to the heat transfer coefficient case, the user is able to include additional methods/correlations as functions to the procedures.

Table 2.4: Implemented methods and correlations for estimation of local frictional pressure drops

Model	Year	Ref.
<i>Single-phase</i>		
Chisholm and Wanniarachchi	1991	[12]
Wanniarachchi et al.	1995	[13]
Martin	1996	[4]
Muley and Manglik	1999	[14]
<i>Evaporation</i>		
Fanning friction factor		
Yan and Lin	1999	[16]
Hsieh and Lin	2002	[48]
Han et.al.	2003	[17]
Hsieh and Lin	2003	[26]
Huang	2012	[25]
Amalfi et.al.	2016	[18]
Zhang et.al.	2017	[19]
Lockhart-Martinelli method		
Palm and Claesson	2006	[22]
Taboas	2012	[8]
Kinetic energy proportionality		
Longo and Gasparella	2007	[47]
<i>Condensation</i>		
Fanning friction factor		
Yan and Lin	1999	[28]
Han et al.	2003	[30]
Zhang et al.	2019	[32]

Void fraction models

Different void fraction models were implemented in the framework to estimate the cross-section void fraction α , namely the ratio between the cross section area occupied by the vapour phase and the total cross section area. The void fraction can be estimated as [49]:

2.1. Plate heat exchanger model

$$\alpha = \left(1 + S_{VL} \frac{1-x}{x} \frac{\rho_V}{\rho_L} \right)^{-1} \quad (2.28)$$

The homogeneous model assumed that the slip ratio S_{VL} is equal to 1, e.g. the vapour and liquid phases flow at the same velocity. Zivi [50] and Smith [51] proposed expressions to estimate S_{VL} , as function of the local vapour quality and vapour and liquid phase density. Rouhani and Axelsson [52] proposed instead a drift flux correlation, in which the void fraction is estimated as function of the liquid and vapour superficial velocities and a drift velocity between the two phases. The implemented models are reported in Table 2.5.

Table 2.5: Implemented correlations for estimation of void fraction

Model	Year	Ref.
Homogeneous model	-	[49]
Zivi	1964	[50]
Rouhani and Axelsson	1969	[52]
Smith	1969	[51]

The void fraction is needed for the computation of two-phase pressure drops. More specifically, it is needed to compute the momentum density ρ_m with Eq. (2.23), as well as the cross section average density ρ , estimated by [53]:

$$\rho = (1 - \alpha)\rho_L + \alpha\rho_V \quad (2.29)$$

2.1.7 Solver for the design problem

The PHE models in design mode are capable to estimate the required heat transfer area at the evaporator and the condenser to meet the design thermal load. Therefore, the inputs required are given by the total heat flow rate and inlet thermodynamic states of both working fluid and secondary fluid.

The geometry of PHEs is determined by the plate size, namely width W and length L . Moreover, the characteristic corrugation patterns in chevron PHEs are defined by the corrugation pitch Λ , corrugation height b and chevron angle β . The plate thickness t determines the trade-off between mechanical strength and wall conductive resistance, while the material influences the value of wall thermal conductivity. Finally, the total number of plates determines the number of channels N_{ch} . In the simulation framework, the manifold (or port) pressure drops are neglected, since they are strictly related to a particular manufactured design. However, the models could be easily extended by the user to account for this type of losses, by introducing a port diameter D_p .

In software for PHE sizing offered by commercial manufacturers (e.g. [54]), the plate size is usually fixed and the number of channels is estimated as output of the design. Different solutions are proposed and 50 kPa maximum pressure drops is a criterion often considered in order to obtain feasible designs. Therefore, it was decided to build a model

Chapter 2. Numerical models

following a similar approach, e.g. for fixed plate geometry, corrugation characteristics and material, the design model is able to estimate the required number of channels to meet the design load. The pressure drops are obtained as model output, thereby the user is able to check the value and tune the input geometrical parameters accordingly.

The flow-chart of the design models is shown in Fig.2.5. A guess values for the number of channels must be provided to the solver for heat transfer and fluid flow, estimating the outlet thermodynamic states of working fluid and secondary side, as well as the total heat flow rate. The convergence to the solution is checked by estimating the relative residual of the total heat flow rate compared to the design value. If the residual is lower than the set tolerance, the solver converged to the set solution. If the tolerance is higher, the derivative of the heat flow rate with respect to the number of channels is estimated and the value of N_{ch} at the next iteration $k + 1$ is updated following the Newton-Raphson method as:

$$N_{\text{ch}}^{k+1} = N_{\text{ch}}^k - \frac{\dot{Q}_{\text{tot}} - \dot{Q}_{\text{design}}}{\frac{d\dot{Q}_{\text{tot}}}{dN_{\text{ch}}}} \quad (2.30)$$

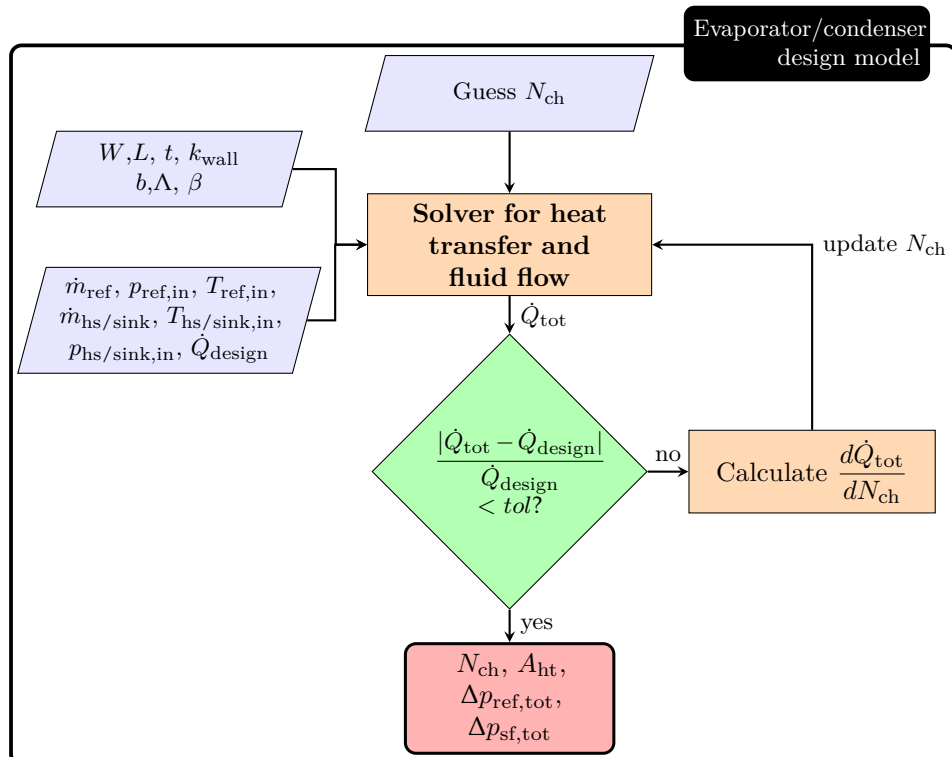


Figure 2.5: Work flow of the design solver

2.2 Coupled HP-PHE off-design model

The coupled HP-PHE evaporator and condenser off-design simulation framework (yellow box in Fig. 1.1) is described in this section. Two different models are presented, with work flow shown in Fig. 2.6 and 2.8. The former is based on the evaluation of evaporator heat transfer and fluid flow in 1D, thereby without accounting for any maldistribution effects. The latter is instead based on a 2D discretization of the evaporator, thus the vapour quality maldistribution is imposed as an input and the mass flow rate distribution of both refrigerant and heat source is found as output of the model. Matlab 2017b *fsolve* built-in algorithm [3] is used in order to solve the governing equation in both cases.

2.2.1 Coupled HP-PHE off-design model without maldistribution effects

If maldistribution effects are neglected (both vapour quality maldistribution and effect of end plates), the off-design model is based on a 1D discretization of the evaporator. Fig. 2.6 shows how the different component models are integrated in an overall solver of the cycle to solve for the operating conditions. First of all, the solver is initialized, e.g. the tolerance are set and the inputs are defined. The inputs are given by the full specified geometry of both evaporator and condenser (preliminary designed with this simulation framework, as in section 2.1.7, or external inputs) and by the control values for off-design operation. In this case, four control variables are specified:

- (i) the degree of superheat at the evaporator outlet, fixed to the design value ΔT_{sh}
- (ii) the subcooling at the condenser outlet, namely a fixed temperature difference is imposed between the outlet refrigerant temperature at the condenser and the inlet heat sink temperature, equal to the minimum pinch point temperature difference $\Delta T_{sc} = \Delta T_{pinch,min}$
- (iii) the suction volume flow rate at the compressor inlet, fixed to the design value $\dot{V}_{eva,out}$
- (iv) the heat sink outlet temperature, fixed to the design value $T_{sink,out-design}$

These four control variables translates into four unknowns, defining the off-design operation of the cycle, namely:

- (i) the total mass flow rate of the refrigerant $\dot{m}_{ref,tot}$
- (ii) the condensation pressure p_{cond}
- (iii) the evaporation pressure p_{evap}
- (iv) the total mass flow rate of the heat sink $\dot{m}_{sink,tot}$

The user is able to modify the solver by releasing one or more of the aforementioned control variables, and subsequently fixing one or more of the four unknowns of the system, depending on the analysed case study. For example, the last constraint was defined in

Chapter 2. Numerical models

light of an application in which a heat pump must provide heat to a district heating network at a fixed temperature level. Another application could however require the definition of an alternative control value. The governing equations solved for the cycle operating parameters are also reported in Fig. 2.6.

In order to estimate the value of the four control variables for different heat pump operating conditions, the *fsolve* solver must be able to solve all the components simultaneously, as shown in the yellow box of Fig. 2.6. The condenser and evaporator are solved by using the solver for heat transfer and fluid flow presented in section ???. The throttling valve is described by an isenthalpic expansion process, while the off-design performance of the compressor is described by means of the formulation by Granryd [55], defined by Eq. (2.31), which relates the isentropic efficiency to a deviating pressure ratio from the design value.

$$\frac{\eta_{is}}{\eta_{is,design}} = \frac{\left(\frac{p_1}{p_2}\right)^{\frac{k-1}{k}} - 1}{\pi_i^{\frac{k-1}{k}} - \frac{k-1}{k} \pi_i^{\frac{-1}{k}} \left(\pi_i - \frac{p_1}{p_2} \right)} \quad (2.31)$$

Here, π_i represents a corrected built-in volume ratio, and k is the exponent of the polytropic describing the compression process. π_i is found by imposing that the correction factor expressed by Eq. (2.31) is equal to one when the pressure ratio is at the design value. This correlation is valid for volumetric compressors with built-in volume ratios. Another approach can be developed and substituted in the framework for case studies requiring the use of other compressor technologies.

The output of the coupled HP-PHE simulation framework is given by the operating conditions of the cycle, as mentioned previously. However, additional outputs are given by the thermodynamic and economic performance indicators of the heat pump. The thermodynamic performance of the heat pump is indicated by the Coefficient of Performance (COP), expressed by Eq. (2.32).

$$COP = \frac{\dot{Q}_{sink}}{\dot{W}_{comp}} \quad (2.32)$$

where \dot{Q}_{sink} is the heat released at the condenser and \dot{W}_{comp} is the work required by the compressor. The economic performance is instead evaluated by the (levelized) specific cost of heat, calculated in €/MWh by Eq.(2.33). This is a function of the total Fuel Cost (CF) of electricity CF_{el}, the income from supplying cold by cooling the heat source CF_{hs}, the Total Capital Investment (TCI), Capital Recovery Factor (CRF) and the yearly production of heat, evaluated by multiplying the condenser load (\dot{Q}_{sink}) by the yearly operating hours (OH). Further details can be found in [56].

$$c_h = \frac{CF_{el} - CF_{hs} + TCI \cdot CRF}{\dot{Q}_{sink} \cdot OH} \quad (2.33)$$

2.2. Coupled HP-PHE off-design model

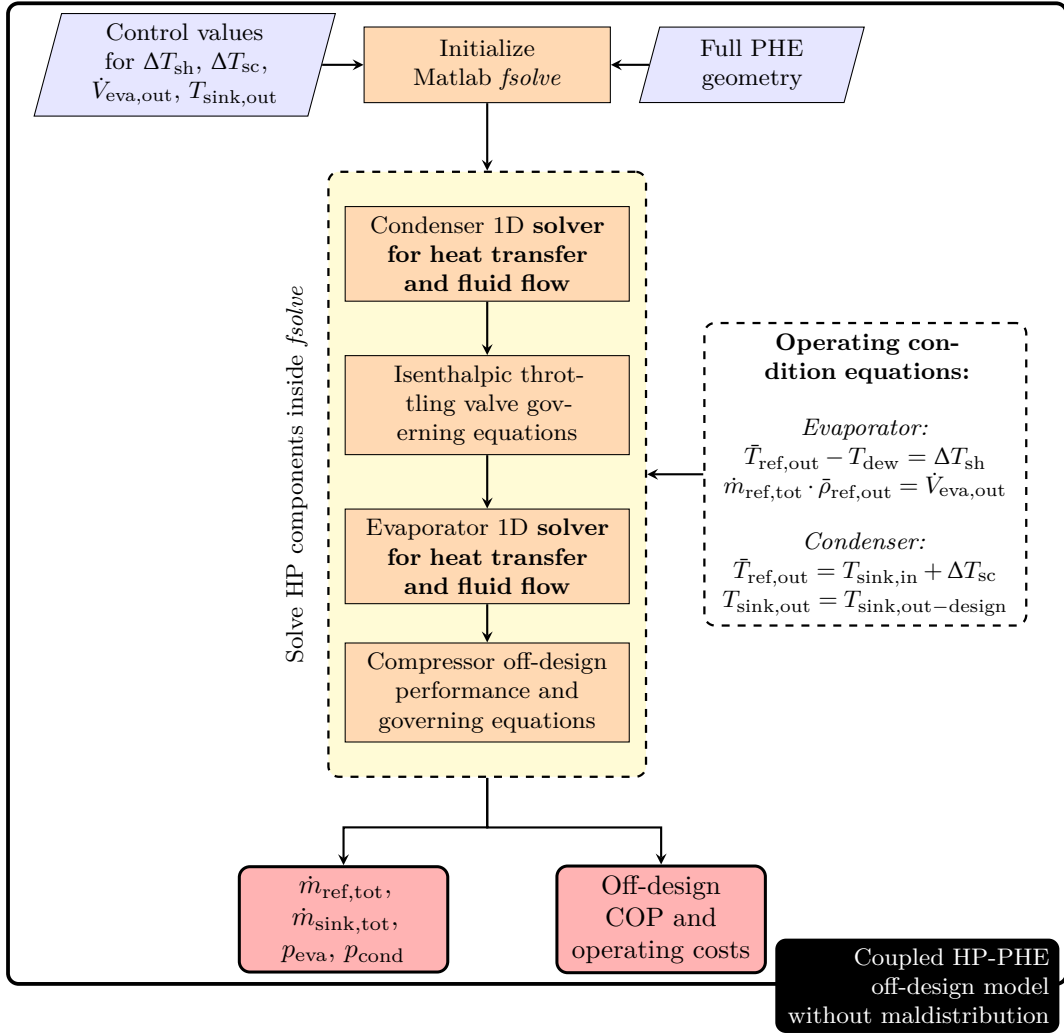


Figure 2.6: Work flow of the coupled off-design heat pump model and PHE performance models without maldistribution effects (1D evaporator model)

2.2.2 Coupled HP-PHE off-design model with maldistribution effects

The coupled HP-PHE simulation framework is able to estimate the performance of heat pumps when maldistribution occurs in the evaporator. Therefore, the maldistribution rate must be imposed as an input parameter.

The model is able to handle linear vapour quality variation between the channels at the PHE inlet. The assumption of linear profile was taken by considering the experimental studies from Vist and Pettersen [57], who showed a monotonic increase/decrease of the vapour phase distribution with increasing distance from the inlet of a manifold distributing two-phase flow into ten different channels.

The maldistribution is therefore defined by a parameter Δx , representing the difference in vapour quality between the outer-most PHE refrigerant channels. The inlet quality at

Chapter 2. Numerical models

the j -th channel, assuming a linear profile, can be therefore calculated by:

$$x_{\text{in}}^{(j)} = x_{\text{in}}^{(1)} + \frac{j-1}{N_{\text{ch,ref}} - 1} \Delta x \quad (2.34)$$

where $x_{\text{in}}^{(1)}$ is the vapour quality of the first channel. The parameter Δx represents the slope of the vapour quality variation. An example of the imposed variation of vapour quality for a case of 11 refrigerant channels and Δx varying between 0 and 0.25 is shown in Fig. 2.7.

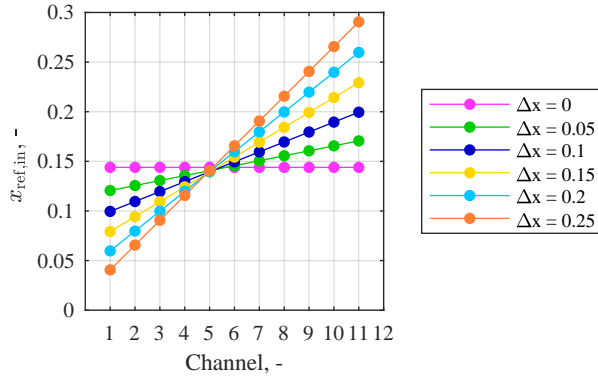


Figure 2.7: Linear vapour quality variation in different PHE channels for different values of Δx

When the parameter Δx is set equal to 0, an uniform vapour quality variation is imposed, thus no liquid/vapour maldistribution effect is considered in the PHE. However, this case allows estimating the effect of end plates, e.g. "*the two outer plates ideally do not transfer heat*" [58]. This means that only interior plates are usually considered to estimate the PHE heat transfer area. The effect of end plates results into a modification of the flow distribution of both refrigerant and secondary fluid, as the outer-most channels transfer a different amount of heat compared to the interior channels. This is taken into account by evaluating the evaporator model in 2D without imposing any variation of the vapour quality, e.g. $\Delta x = 0$.

Fig. 2.8 shows the integration of the component models for the solution of both the heat pump operating conditions and the mass flow distribution inside the evaporator. In this case, the 2D evaporator solver for heat transfer and fluid flow must be employed. The procedure is similar to the one showed in Fig. 2.6 for the estimation of the off-design heat pump performance without considering maldistribution effects. The main differences are given by the additional input of the maldistribution rate, as well as by the additional unknowns and equations. In fact, a total of $N_{\text{ch,ref}} + N_{\text{ch,hs}} + 1$ unknowns is added

2.2. Coupled HP-PHE off-design model

to the four operating variables defined by the control values. These are given by the mass flow rate distribution of the refrigerant in the $N_{\text{ch,ref}}$ channels, the mass flow rate distribution of the heat source in the $N_{\text{ch,hs}}$ channels and the inlet vapour quality in the first channel x_{in}^1 (the vapour quality at the other channels is then estimated by Eq. (2.34)). The additional required governing equations are reported in Table 2.6. The first three equations ensure mass conservation in the manifold for both refrigerant, heat source and vapour phase. The latter $N_{\text{ch,ref}} - 1$ and $N_{\text{ch,hs}} - 1$ equations impose equalization of the outlet pressure for the different channels, for both refrigerant and heat source. Note that manifold pressure drops are neglected, thereby the inlet pressure is considered to be the same for the different channels, despite there is a contribution of manifold pressure drops decreasing the inlet pressure of the working fluids in those channels which are farthest from the inlet. However, Li and Hrnjak [59] showed that for single-phase flow this contribution is negligible for PHE with 10 plates, very small for PHE with 50 plates and starts becoming relevant only for 100 plates.

Table 2.6: Evaporator flow distribution equations

Mass conservation in manifold		
<i>Refrigerant</i>	<i>Heat source</i>	<i>Refrigerant vapour</i>
$\sum_{j=1}^{N_{\text{ch,ref}}} \dot{m}_{\text{ref}}^{(j)} = \dot{m}_{\text{ref,tot}}$	$\sum_{j=1}^{N_{\text{ch,hs}}} \dot{m}_{\text{hs}}^{(j)} = \dot{m}_{\text{hs,tot}}$	$\sum_{j=1}^{N_{\text{ch,ref}}} \dot{m}_{\text{ref}}^{(j)} \cdot x_{\text{ref,in}}^{(j)} = \dot{m}_{\text{ref,tot}} \cdot x_{\text{ref,in}}$
Outlet pressure equalization		
<i>Refrigerant</i>	<i>Heat source</i>	
$\sum_{i=1}^n \Delta p_{\text{ref}}^{(j,i)} = \sum_{i=1}^n \Delta p_{\text{ref}}^{(j+1,i)},$ $j = 1, \dots, N_{\text{ch,ref}} - 1$	$\sum_{i=1}^n \Delta p_{\text{hs}}^{(j,i)} = \sum_{i=1}^n \Delta p_{\text{hs}}^{(j+1,i)},$ $j = 1, \dots, N_{\text{ch,hs}} - 1$	

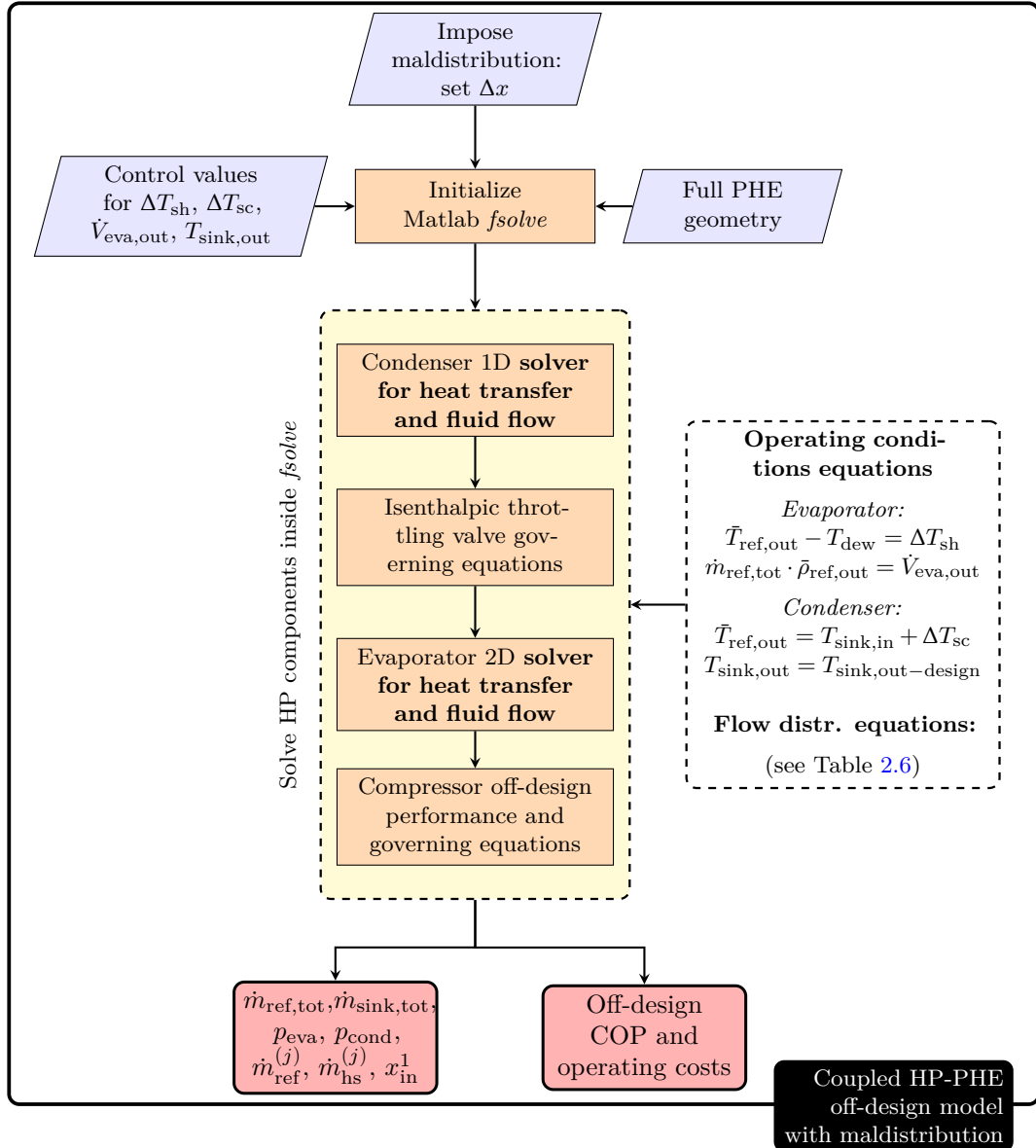


Figure 2.8: Work flow of the coupled off-design heat pump model and PHE performance models with maldistribution effects (2D evaporator model)

3 Validation and verification

This chapter presents the verification of the flow distribution solver compared to a model from literature, and the validation of the PHE solver for heat transfer and fluid flow against experimental data. As suggested by Vakili-Farahani et al. [44], the deviation between the model results and the experimental data (or the reference model from literature) is reported for all cases in terms of the mean relative error δ and mean absolute error $|\delta|$, estimated by Eq.(3.1) and (3.2), respectively, in percentage points.

$$\delta = \frac{1}{N} \cdot \sum_{i=1}^N \left(\frac{\theta_{\text{model}} - \theta_{\text{exp}}}{\theta_{\text{exp}}} \right) \cdot 100 \quad (3.1)$$

$$|\delta| = \frac{1}{N} \cdot \sum_{i=1}^N \left| \frac{\theta_{\text{model}} - \theta_{\text{exp}}}{\theta_{\text{exp}}} \right| \cdot 100 \quad (3.2)$$

θ represents the compared quantity, i.e. total heat flow rate and refrigerant total pressure drops, and N represents the number of the considered experimental data points. For the comparison with experimental data, the models were used in rating mode (see section 2.1). The model received as inputs the full PHE geometry and inlet thermodynamics of both fluids, as gave the total heat flow rate, pressure drops and outlet thermodynamics as outputs. Experimental heat flow rate and refrigerant pressure drop (when available from measurements) were then used to evaluate the model accuracy. For the flow distribution solver verification, the reference was given by the quantity evaluated by the reference model.

3.1 Flow distribution solver verification

The flow distribution solver was verified against the results of the model presented in [59]. Li and Hrnjak [59] developed an experimentally validated model to solve single-phase flow distribution in PHEs. The model was built using a similar approach compared to the present model, i.e. by imposing equations to ensure global conservation of mass and *identical pressure drop* for each flow path.

Chapter 3. Validation and verification

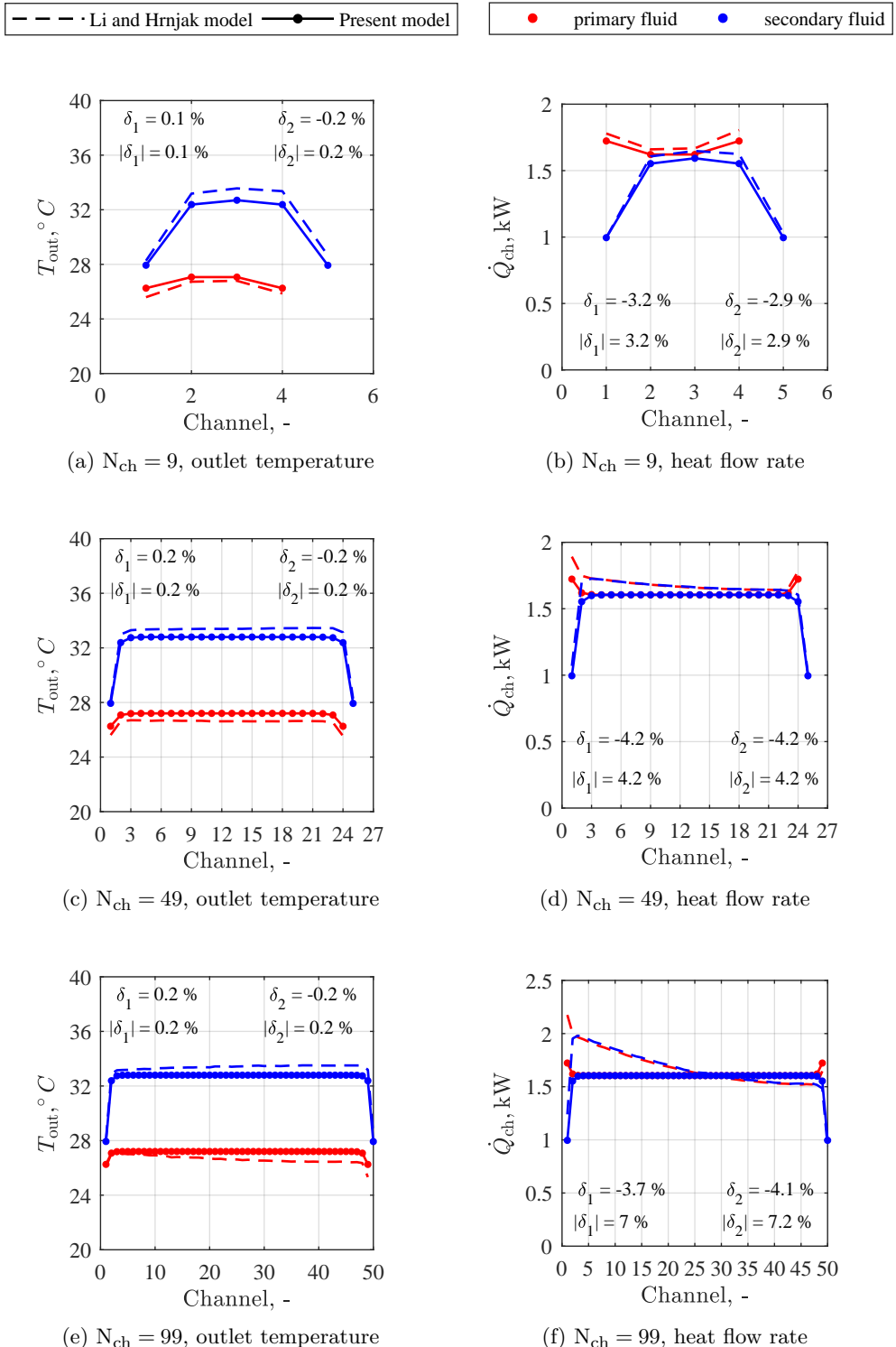


Figure 3.1: Comparison between the results of the present model and the results of the model by Li and Hrnjak [59]

3.2. Comparison with experimental data: evaporation data from DTU

Li and Hrnjak [59] accounted for frictional, gravity and manifold pressure drop, while they neglected the acceleration contribution. The manifold pressure drop is on the contrary neglected in the present model.

The outlet temperature in each channel for both primary and secondary fluid, as well as the heat flow rate exchanged by the channels, were compared with the results of the model by Li and Hrnjak for three PHEs, with a fixed plate geometry and different number of channels. Hot and cold water streams were used as primary and secondary fluid, respectively. By increasing the number of channels, the manifold pressure drop increases, thus enhancing the difference of the inlet pressure between the outermost channels. Therefore, it is expected to have larger discrepancies between the model results for higher number of channels.

Fig. 3.1 reports the result of the verification. The deviations between the models were quantified in terms of mean relative error and mean absolute error, thus computed by Eq.(3.1) and (3.2). The two models showed an overall satisfactory agreement with the highest deviation for both outlet temperature and heat flow rate achieved in the case of $N_{ch} = 99$. The highest deviation for temperature was found to be as low as 0.2 %.

In all cases, the present model overestimated the outlet temperature of the primary fluid (red line, hot fluid), while the outlet temperature of the cold water stream (blue line) was underestimated. This was due to a general underestimation of the heat flow rate exchanged between the channels. The highest deviation on heat flow rate was found in the case of $N_{ch} = 99$, with mean absolute errors of 7.0 % and 7.2 % on the heat flow rates in the hot and cold fluid channels, respectively. The mean relative errors were found to be -3.7 % and -4.1 %, thus the heat flow rate was overestimated or underestimated depending on the channel.

It is noted that the deviation for temperature was calculated for the temperature in K, even though Fig. 3.1 (a), (c) and (e) report the temperature in °C. Moreover, the results showed that it is acceptable to neglect manifold pressure drops when the number of channels is not too large, and that errors below 10 % are obtained even in the case of 99 total channels.

3.2 Comparison with experimental data: evaporation data from DTU

A total of 316 flow boiling data from the experimental study by Zhang et al. [19], for R134a (106 points), R1234yf (91 points) and R1234ze(E) (119 points) were used. The study was carried out in the laboratory of DTU Mechanical Engineering. The data included information on both total heat flow rate and refrigerant pressure drop. In the PHE model, the heat transfer coefficient was estimated locally by applying the correlation by Amalfi et al. [18], while the frictional pressure drop was estimated by calculating the Fanning friction factor according to Yan and Lin [16]. The comparison was carried out using the models discretized in both 1D and 2D. The 2D model was applied together with the flow distribution solver by imposing an uniform vapour quality distribution at the inlet of the PHE channels, thereby solely accounting for the effect of end plates.

Chapter 3. Validation and verification

Fig. 3.2 reports the comparison of the total heat flow rate and total refrigerant pressure drop for both the 1D and 2D model, considering all the experimental data points. Table 3.1 reports the deviations for each working fluid separately. The 1D model slightly overestimated the experimental values, with a relative deviation of +4.3 %, while in the 2D case the deviation was -2.3 %. The difference is likely due to the effect of end plates, which slightly degrades the heat transfer performance of the evaporator and is considered solely in the 2D model. [?] found that this effect is not negligible for configurations with less than 20 channels, and the experimental study was carried out on a PHE configuration

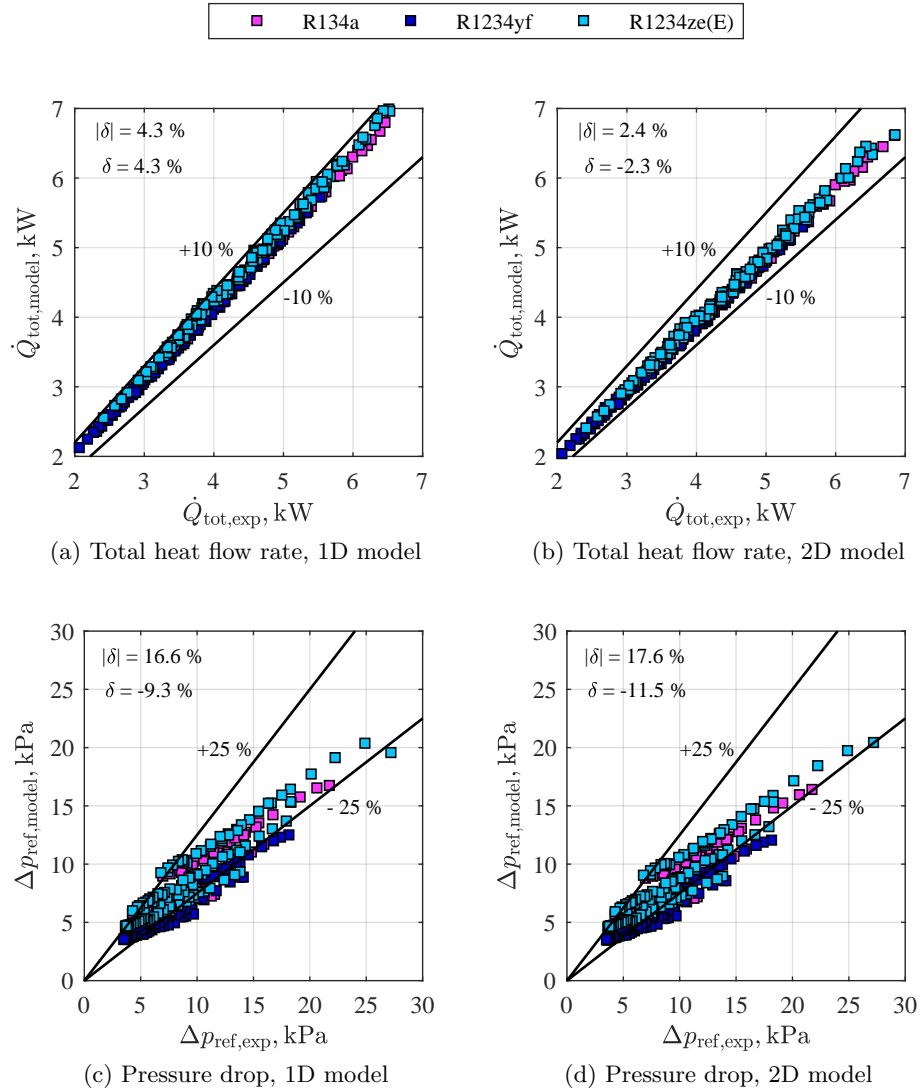


Figure 3.2: Comparison of simulated data points vs. experimental data for the (a), (b) total heat flow rate, and (c), (d) total refrigerant pressure drop

3.3. Comparison with experimental data: condensation data from DTU

Table 3.1: Deviations between experimental data and results of the evaporator model using 1D and 2D discretization (DTU data)

Working fluid	1D model				2D model			
	Heat flow rate		Pressure drop		Heat flow rate		Pressure drop	
	δ	$ \delta $	δ	$ \delta $	δ	$ \delta $	δ	$ \delta $
R134a	3.6	3.6	-6.5	14.7	-2.9	2.9	-8.6	15.6
R1234yf	2.9	2.9	-21.1	21.2	-2.9	2.9	-22.9	23.0
R1234ze(E)	6.1	6.1	-2.8	14.6	-1.3	1.5	-5.3	15.3
Overall	4.3	4.3	-9.3	16.6	-2.3	2.4	-11.5	17.6

with 7 channels in total [19].

R1234ze(E) resulted in the highest deviation for the 1D model, i.e. 6.1 % overestimation of the total heat flow rate. The discrepancy reduced however down to -1.3 % for the 2D model, resulting in the best match with the experimental data compared to the two other working fluids. This might be due to a higher sensitivity of R1234ze(E) to the effect of end plates compared to the other working fluids, hence leading to a higher deviation from experimental data when the effect was neglected with the 1D model.

Higher errors were reported for refrigerant pressure drop for all the fluids, with a general underestimation of the value calculated by the model, with the errors equal to -9.3 % and -11.5 % for the 1D and 2D models, respectively. R1234yf resulted in the highest deviation, while R134a and R1234ze(E) presented similar matches. It is noted that Zhang et al. [19] reports the maximum uncertainty on the measured pressure drop and heat flow rate equal to 6.6 % and 2.8 %, respectively. Therefore, the model results and the experimental data showed an overall good match, with maximum deviations in the same order of magnitude of the experimental uncertainty.

3.3 Comparison with experimental data: condensation data from DTU

Experimental data from the campaign by Zhang et al. [32] for R134a, R1234ze(E), R245fa and R1233zd(E) were used. The data were collected in the same test-rig of the evaporation data of section 3.2. The correlations by Zhang et al. [32] were applied to compute the heat transfer coefficient and two-phase friction factor. For the condenser, only the 1D discretization approach was implemented and thus compared against experimental data. Fig. 3.3 reports the results in terms of total heat flow rate and total pressure drop of the refrigerants. The model underestimated overall the total heat flow rate with mean relative and mean absolute errors equal to -8.4 % and 9.9 %, respectively. The model underestimated the results for all working fluids with the exception of R245fa, which presented the best match with a slight mean overestimation of 4.1 %. On the other hand, the total pressure drop was overall overestimated by the model, with mean relative and mean absolute errors equal to 15.6 % and 20.6 %, respectively. The model overestimated

Chapter 3. Validation and verification

the results for all working fluids, with R245fa showing the lowest mean relative error equal to 6.4 %, yet resulting in a higher absolute value of 16.6 %.

Zhang et al. [32] reported the maximum uncertainty on the experimental total heat flow rate and frictional pressure drop, as 4.1 % and 15.2 %, respectively. Therefore, similarly to the results of the evaporator model, the model results and the experimental data showed an overall good match, with maximum deviations in the same order of magnitude of the experimental uncertainty.

Table 3.2: Deviations between experimental data and results of the model

Working fluid	Heat flow rate		Pressure drop	
	δ %	$ \delta $ %	δ %	$ \delta $ %
R134a	-6.8	6.8	20.3	25.3
R1234ze(E)	-16.2	16.2	11.6	16.3
R245fa	4.1	4.7	6.4	16.6
R1233zd(E)	-9.6	9.6	23.7	23.7
Overall	-8.4	9.9	15.6	20.6

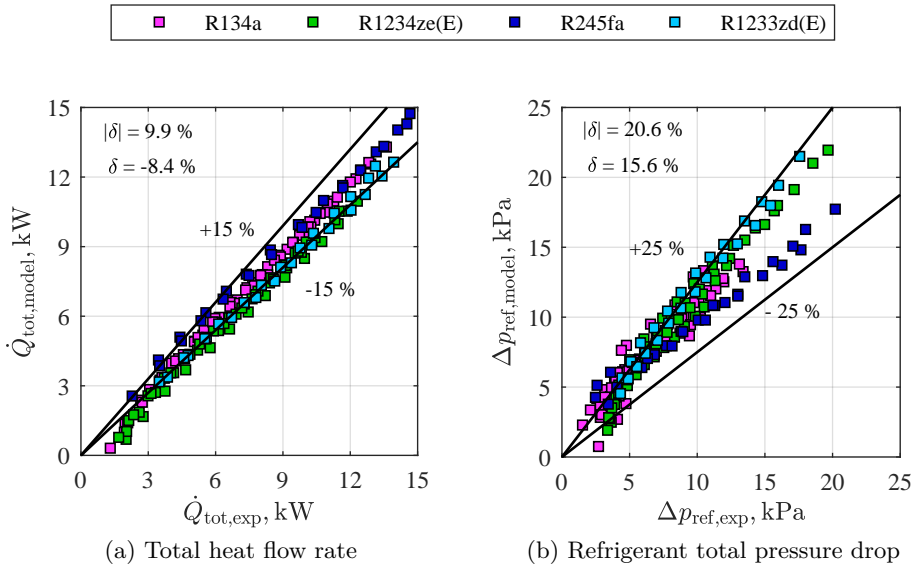


Figure 3.3: Comparison of simulated data points vs. experimental data for the (a) total heat flow rate and (b) total refrigerant pressure drop

3.4 Solution sensitivity to model tolerances

A sensitivity study of the PHE models solutions for different values of model tolerances was carried out for the solvers of heat transfer and fluid flow, in both 1D and 2D for the

3.4. Solution sensitivity to model tolerances

evaporator, and 1D for the condenser. The same test case was chosen for the evaporator 1D and 2D models, so that the two solutions could be compared.

Fig. 3.5 shows the results of the sensitivity of the evaporator 1D and 2D models. Fig. 3.5 (a) and (d) report the convergence rates, e.g. how the error (estimated as explained in Fig. 2.4) decreases with increasing number of model iterations, for the three iteration variables wall temperature, refrigerant and secondary fluid pressure drops. Fig. 3.5 (b) and (e) show the total estimated heat flow rate as function of the chosen tolerance, while Fig. 3.5 (c) and (f) report the trends of the refrigerant total pressure drops. It can be observed that there is a slight discrepancy between the result of the 1D and 2D models, due to the neglected effect of end plates in the 1D case. It can be observed that the solution becomes stable for tolerances values lower than 10^{-4} . We thus recommend the use of a tolerance not higher than 10^{-4} when using the evaporator models. In particular, since equalization of pressure drops in the different evaporator channels determines some of the governing equations of the flow distribution solver, it is recommended to choose a tolerance value for the evaporator 2D model ensuring the stability of the refrigerant pressure drops as output of the model. Fig. 3.4 reports analogous results for the condenser case. Similarly to the evaporator, a tolerance of at least 10^{-4} must be chosen to ensure the convergence to the solution. In the work presented in [1], a tolerance of 10^{-5} was selected for both evaporator and condenser models.

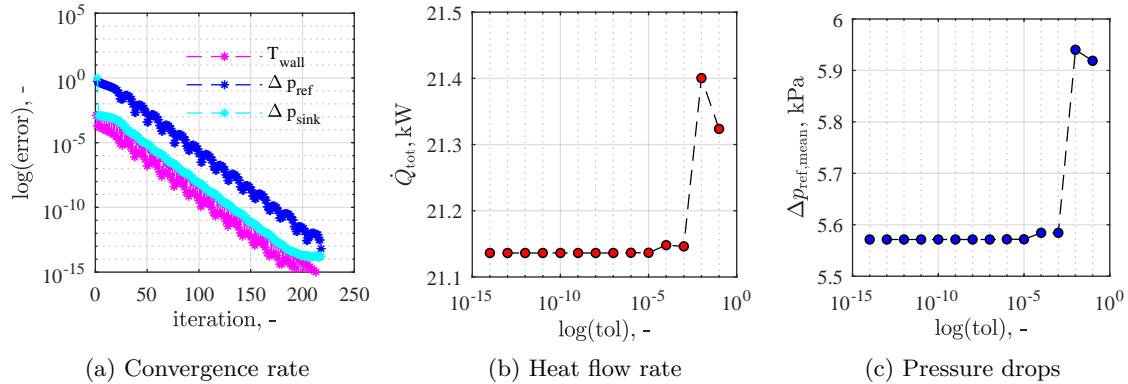


Figure 3.4: (a) Condenser model convergence as function of the iteration number; (b,c) Sensitivity of the condenser model outputs from the set tolerance

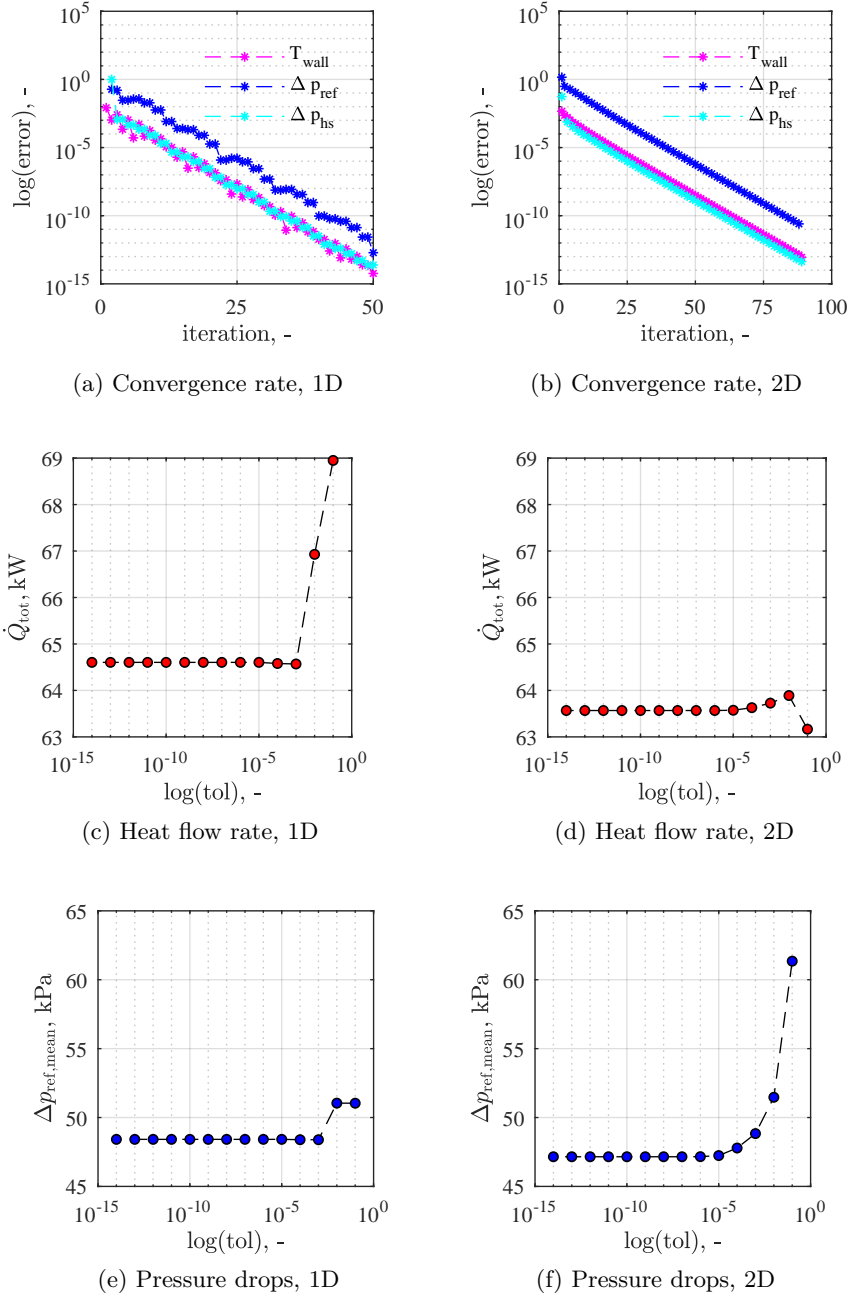


Figure 3.5: (a,b) Evaporator models convergence as function of the iteration number; (c,d,e,f) Sensitivity of the evaporator models outputs from the set tolerance

3.5. Grid independence study

3.5 Grid independence study

In [60] a grid independence study is defined as a "*procedure of successive refinement of an initially coarse grid until certain key results do not change*". The user is thus encouraged to carry out a grid independence study before using the numerical models, in order to select appropriate number of CVs for the discretization. In this section, an example is presented for the same test cases used for the sensitivity study to model tolerances. Fig. 3.7 shows the results for the evaporator 1D and 2D models, while Fig. 3.6 reports the results for the condenser model. The results are presented in terms of total PHE heat flow rate and total refrigerant pressure drops as function of the number of elements used for the discretization. Both heat flow rate and pressure drops were considered as the key output of the solver for heat transfer and fluid flow. Note that in the 2D model the discretization among the different channels is always carried out by diving for a number of elements equal to the number of channels, while the discretization along the fluid flow direction can be subjected to changes and thus analysed in the grid independence study. Both Fig. 3.7 and 3.6 report dotted lines in which the tolerance bounds (set to 10^{-5}) are given for the solution found using $n = 250$. The bounds give thus an idea on what is the magnitude of the solution variation for the different cases. It can be for example observed that the condenser model is much more sensitive to grid refinement compared to the evaporator model, since the tolerance bounds are not detectable in Fig. 3.6. It is therefore recommended to choose a number of CVs equal to 100, from where the solutions becomes stable. On the other hand, both the axis scale and the tolerance bounds of the evaporator grid independence study shown in Fig. 3.7, show that the evaporator model outputs are less sensitive to the number of CVs. Choosing 50 elements ensure the convergence of the solution to values that are almost within the tolerance bounds. In [1], $n = 50$ was chosen for the evaporator models in 1D and 2D, while $n = 110$ was chosen for the condenser model.

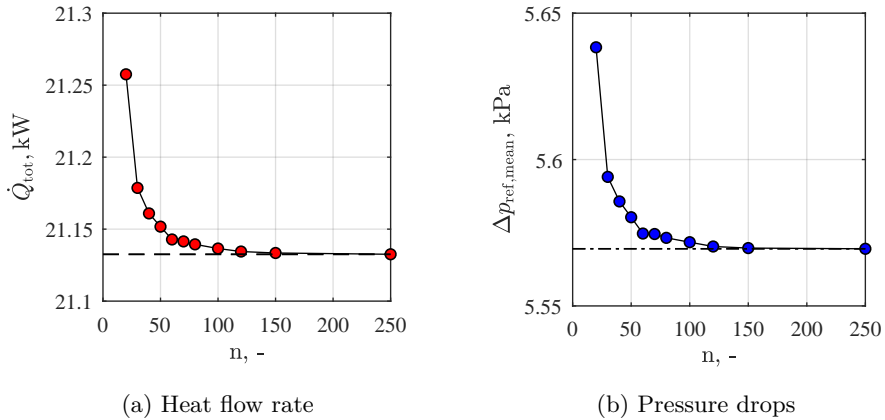


Figure 3.6: Grid independence study for the condenser 1D model

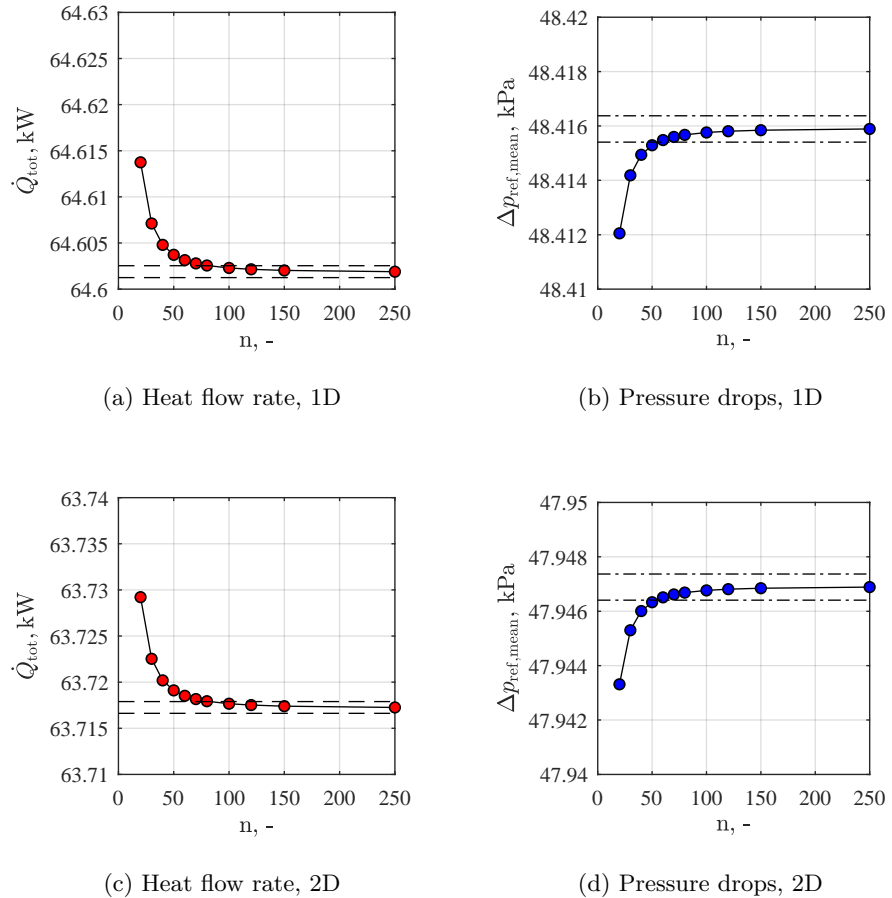


Figure 3.7: Grid independence study for the evaporator 1D and 2D models

4 User guide

4.1 System requirements

The models were implemented in Matlab 2017b [3]. The installation of the *Optimization toolbox* is required in order to use the *fsolve* algorithm to solve the system of non-linear equations.

Medium properties can be calculated by means of Refprop [61] or CoolProp [62]. In both cases, fluid properties are called by means of the so-called *low level interface* (LLI) of Matlab via CoolProp. The use of the interface requires the installation of Python [63], with the packages *numpy* and *coolprop* installed. It is possible to download the wrappers at <https://github.com/CoolProp/CoolProp/tree/master/wrappers/MATLAB>. The reader is referred to the guide on how to use the *low level interface* of CoolProp [64]. The function needed to run the LLI is named *AbstractState*. Therefore, it is important to include this function in the Matlab work directory. In order to choose if medium properties are estimated calling CoolProp or Refprop, two different *backends* can be used, namely '*HEOS*' and '*REFPROP*' respectively.

4.2 Model structure

The models are divided in two folders, namely *PureFluidsSimulations* and *Mixtures-Simulations*. This is done in order to avoid unnecessary property calls for the case of pure fluids. In fact, the models collected in *MixturesSimulations* can easily run for pure fluids by imposing the mass fraction of one of the component to be equal to zero. However, mixture calculations require the estimation of vapour and liquid properties in each CVs, since there is a varying composition of the liquid and vapour phase during both evaporation and condensation. On the other hand, the saturation properties of pure fluids can be easily estimated as function of the saturation pressure (temperature), thereby avoiding computationally expensive fluid properties calls in each CV. For this reason, the two simulation frameworks are divided in two separate folders. The structure is however completely analogous and it will be therefore illustrated only for one of the cases.

The models are structured as shown in Fig. 4.1. The overall structure shows the main scripts and all the folders containing the scripts necessary to run the models. The two Matlab scripts *Call_Maldistribution_2D* and *Call_OperationalModel_1D* run the overall

Chapter 4. User guide

simulation framework, as reproduced in Fig. 4.1. The former runs the maldistribution studies when a certain liquid/vapour maldistribution is defined by the maldistribution parameter Δx , while the latter runs the operational model with both evaporator and condenser solely discretized in 1D.

The PHE scripts, as shown in Fig. 4.1, are collected under the three folders *1D_modelCOND*, *1D_modelEVA* and *2D_modelEVA*. *Evaporator_Design_1D* and *Condenser_Design_1D* are the functions for the design of the evaporator and condenser, respectively. The cycle scripts are collected under the folders *Cycle*, for cycle design and off-design solvers with and without maldistribution. Moreover, the folder *Economy* collects the functions needed to estimate the heat pump investment and operating costs for the data center case study analysed in [1]. These functions can be easily replaced by user made functions if the case study is changed. The folder *Correlations* collect all the experimental correlations implemented in the simulation framework and presented in Chapter 2.1.6. The folder *FunctionsHTC_DP* collects the Matlab functions created in order to estimate the single-phase and two-phase heat transfer coefficients and pressure drops. These are particularly needed in order to smooth the heat transfer coefficient and frictional pressure drops transition between single-phase and two-phase, so that continuity is ensured and the model convergence is improved.

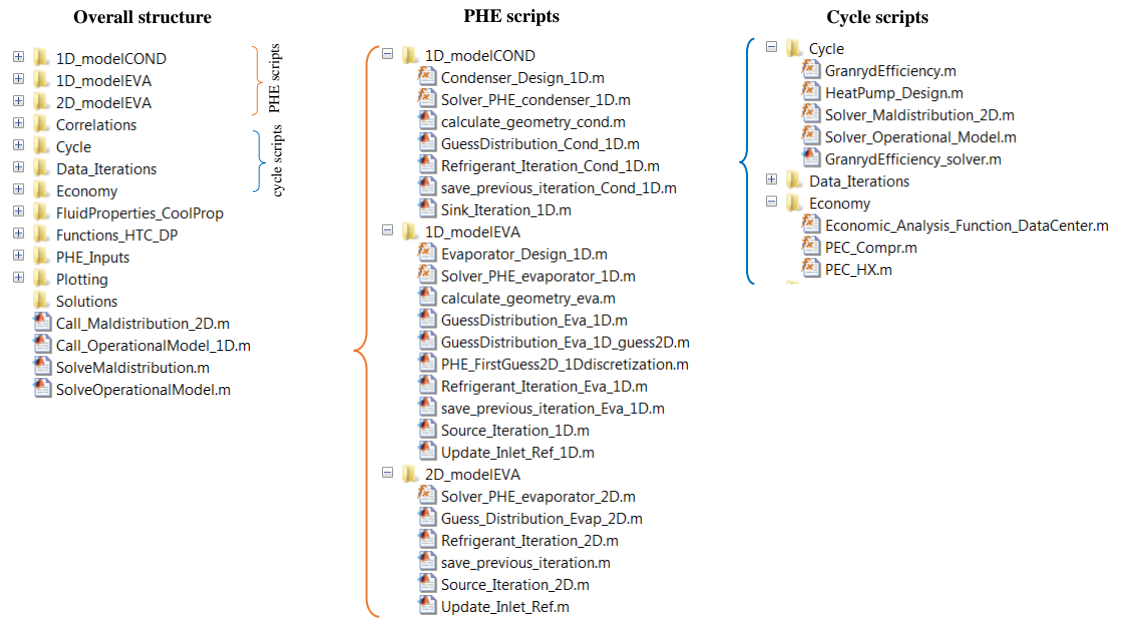


Figure 4.1: Structure of the simulation framework

4.2.1 Model inputs

The inputs are organized and divided among the following Matlab *struct* variables:

- *model* contains the inputs needed for the solvers for the PHEs and the heat pump. The tolerances can be set, as well as the number of maximum iterations and the step for the Newton-Raphson solvers. Moreover, the vapour quality limits at which smoothing between two-phase and single-phase starts for the computation of heat transfer coefficients and frictional pressure drops can be specified.
- *eva* and *cond* contain information about evaporator and condenser design. The geometry to be used as input for the design can be specified through the substructure *geometry*. If the design models are run, the user must specify the plate size and corrugation parameters, as well as material and refrigerant/secondary fluid flow direction. The number of channels is subsequently estimated by the design models and inserted in the *geometry* structure together with heat transfer area and design pressure drops. On the other hand, if the user wish to use solely the coupled heat pump-PHE off-design model for maldistribution studies, he/she can avoid to run the evaporator and condenser designs and define the total geometry as inputs in the aforementioned structures.
- *prediction_methods* contains the choice of the experimental correlations. The user is able to choose among all the correlations implemented in the framework. Alternatively, a different prediction method could be directly implemented and substituted in the framework. In this case, the functions collected in the folder *Functions_HTC_DP* must be modified in order to include the additional correlation.
- *fluids* collects the CoolProp objects needed to estimate the fluid properties for refrigerant (pure fluid or mixture), heat source and heat sink. These objects are passed to the different functions of the simulation framework by means of the *fluids* struct.
- *ref*, *source* and *sink* contain the defined inputs related to refrigerant, heat source and heat sink, for the heat pump design. The simulation framework was built for the case study presented in [1], thus the heat flow rate at the heat source *source.Qdot_design* is specified as input. Other inputs include the sink and source inlet and outlet temperature and pressure, minimum pinch temperature difference in the heat exchangers, minimum refrigerant superheat.
- *comp* and *economy* collect the inputs for the compressor, e.g. isentropic and motor efficiencies, and the necessary inputs for the economic analysis, e.g. lifetime of the plant, effective interest rate, operating hours, specific cost of heat and electricity.

4.2.2 Model outputs

The outputs are collected among the following Matlab *struct* variables:

Chapter 4. User guide

- *HP_DESIGN* collects the outputs of the heat pump design model, among which refrigerant mass flow rate, evaporating and condensing pressures, COP, suction volume flow rate at the compressor inlet, heat flow rates, compressor work, outputs of the economic analysis.
- *EVA_DESIGN* and *COND_DESIGN* collect the output of the evaporator and condenser design models, respectively. In particular, the total required number of channels, the total heat transfer area and the refrigerant pressure drops at design conditions are collected as outputs.
- *OUTPUT_OFF_2D* collects the results of maldistribution studies. If the simulation framework is run for different values of Δx , the struct collects the different cases using different indexes i *OUTPUT_OFF_2D*(i).
- *OUTPUT_OFF_1D* collects the results of the coupled heat pump-PHEs off-design model with no liquid/vapour maldistribution imposed at the inlet of the evaporator.

Final remarks

Author contributions

Roberta Mancini was responsible for the development, implementation, testing and documentation of the numerical models. Benjamin Zühlendorf developed a first version of the function to design the heat pump cycle, which was then modified and integrated in the framework by Roberta Mancini. Benjamin Zühlendorf and Brian Elmegaard contributed by discussions throughout the process. All authors have given approval to the final version of the numerical models.

Acknowledgements

This research project is financially funded by The Danish Council for Strategic Research in Sustainable Energy and Environment, under the project title **THERMCYC**: Advanced Thermodynamic Cycles Utilizing Low Temperature Heat Sources. The support is gratefully acknowledged.

Postdoc Ji Zhang at DTU Thermal Energy is acknowledged for kindly providing the data for the validation of condenser and evaporator model, as well as useful discussion and inputs.

Roberta Mancini would like to acknowledge Research Scientist Dr. Vikrant C. Aute at University of Maryland for useful discussions and inputs during the development of the plate heat exchanger 2D model and the maldistribution studies.

Bibliography

- [1] R. Mancini, B. Zühlsdorf, V. Aute, W. Brix Markussen, and B. Elmegaard. Performance of heat pumps with pure and mixed refrigerants with maldistribution effects in plate heat exchanger evaporators. *submitted to International Journal of Refrigeration*, 2018.
- [2] B. Zühlsdorf. Numerical models for the design and analysis of heat pumps with zeotropic mixtures, 2018. URL <https://figshare.com/s/575b3a3760275aee119e>.
- [3] Mathworks. Matlab 2017b, 2017. URL <https://www.mathworks.com>.
- [4] Holger Martin. A theoretical approach to predict the performance of chevron-type plate heat exchangers. *Chemical Engineering and Processing: Process Intensification*, 35(4):301–310, 1996. ISSN 02552701. doi: 10.1016/0255-2701(95)04129-X.
- [5] José M. Corberán, P. F. De Córdoba, José González, and Francisco Alias. Semi-explicit method for wall temperature linked equations (sewtle): A general finite-volume technique for the calculation of complex heat exchangers. *Numerical Heat Transfer, Part B: Fundamentals*, 40(1):37–59, 2001. ISSN 10407790. doi: 10.1080/104077901300233596.
- [6] José M Corberán, P. Fernández de Córdoba, S. Ortuno, V. Ferri, and P. Montes. Modelling of compact evaporators and condensers. *Computational Studies*, 3:487–496, 2000.
- [7] Radia Eldeeb, Vikrant Aute, and Reinhard Radermacher. An Improved Approach for Modeling Plate Heat Exchangers Based on Successive Substitution in Alternating Flow Directions. In *Proceedings of the International Refrigeration and Air Conditioning Conference, Purdue university, US*, 2016. ISBN 3014058726.
- [8] Francisco Táboas, Manel Vallès, Mahmoud Bourouis, and Alberto Coronas. Assessment of boiling heat transfer and pressure drop correlations of ammonia/water mixture in a plate heat exchanger. *International Journal of Refrigeration*, 35(3):633–644, 2012. ISSN 01407007. doi: 10.1016/j.ijrefrig.2011.10.003.
- [9] L Silver. Gas cooling with aqueous condensation. *Industrial Chemist and Chemical Manufacturer*, 23(269):380–386, 1947.

Bibliography

- [10] KJ Bell and MA Ghaly. An approximate generalized design method for multicomponent/partial condenser. *AIChE Symposium Series*, 69:72–79, 1973.
- [11] R. G. Sardesai, R. A.W. Shock, and D. Butterworth. Heat and mass transfer in multicomponent condensation and boiling. *Heat Transfer Engineering*, 3(3-4): 104–114, 1982. ISSN 15210537. doi: 10.1080/01457638108939589.
- [12] D. Chisholm and A. S. Wanniarachchi. Layout of plate heat exchangers. *ASME/JSME Thermal Engineering Proceedings*, 4:433–438, 1991.
- [13] A S Wanniarachchi, U Ratnam, B E Tilton, and K Dutta-Roy. Approximate correlation for chevron-type plate heat exchangers. In *30th National heat transfer conference*, volume 12, 1995. ISBN 079181713X.
- [14] A Muley and R.M. Manglik. Experimental study of turbulent flow heat transfer and pressure drop in a plate heat exchanger with chevron plates. *Journal of heat transfer - transactions of the ASME*, 121(1):110–117, 1999.
- [15] G.N. Danilova, V.M. Azarskov, and B.B. Zemskov. Teploobmen v plastinchatihispariteljan razichnole geometri (Heat transfer in plate evaporators of different geometry) (in Slovenian). *Kholodilnaya Tekhnika*, 4:25–31, 1981.
- [16] Y Yan and T.F. Lin. Evaporation heat transfer and pressure drop of refrigerant R134a in Plate Heat Exchanger. *Journal of Heat Transfer-Transactions of the Asme*, 121(1):118–127, 1999. doi: 10.1115/1.2825924.
- [17] Dong Hyouck Han, Kyu Jung Lee, and Yoon Ho Kim. Experiments on the characteristics of evaporation of R410A in brazed plate heat exchangers with different geometric configurations. *Applied Thermal Engineering*, 23(10):1209–1225, 2003. ISSN 13594311. doi: 10.1016/S1359-4311(03)00061-9.
- [18] Raffaele L. Amalfi, Farzad Vakili-Farahani, and John R. Thome. Flow boiling and frictional pressure gradients in plate heat exchangers. Part 2: Comparison of literature methods to database and new prediction methods. *International Journal of Refrigeration*, 61:185–203, 2016. ISSN 01407007. doi: 10.1016/j.ijrefrig.2015.07.009.
- [19] Ji Zhang, Adriano Desideri, Martin Ryhl Kærn, Torben Schmidt Ommen, Jorrit Wronski, and Fredrik Haglind. Flow boiling heat transfer and pressure drop characteristics of R134a, R1234yf and R1234ze in a plate heat exchanger for organic Rankine cycle units. *International Journal of Heat and Mass Transfer*, 108:1787–1801, 2017. ISSN 00179310. doi: <https://doi.org/10.1016/j.ijheatmasstransfer.2017.01.026>.
- [20] K Stephan and M Abdelsalam. Heat transfer correlations for natural convection boiling. *International Journal of Heat and Mass Transfer*, 23:73–87, 1980. doi: 10.1016/0020-7233(80)90017-9.
- [21] M.G. Cooper. Heat flow rates in saturated nucleate pool boiling - a wide ranging examination using reduced properties. *Advances in Heat Transfer*, 16:59–156, 1984.

Bibliography

- [22] Björn Palm and Joachim Claesson. Plate heat exchangers: Calculation methods for single and two-phase flow. *Heat Transfer Engineering*, 27(4):88–98, 2006. ISSN 01457632. doi: 10.1080/01457630500523949.
- [23] Dieter Gorenflo. Pool boiling. In Peter Stephan, editor, *VDI Heat Atlas Second Edition Chapter H2*, chapter H2, pages 757–792. Springer Berlin Heidelberg, 2010.
- [24] Dieter Steiner. Flow boiling, an introduction. In Peter Stephan, editor, *VDI Heat Atlas Second Edition Chapter H3 - 3.1*, chapter H3, pages 793–800. Springer Berlin Heidelberg, 2010. ISBN 9783540778769.
- [25] Jianchang Huang, Thomas J. Sheer, and Michael Bailey-Mcewan. Heat transfer and pressure drop in plate heat exchanger refrigerant evaporators. *International Journal of Refrigeration*, 35(2):325–335, 2012. ISSN 01407007. doi: 10.1016/j.ijrefrig.2011.11.002.
- [26] Y.Y. Hsieh and T.F. Lin. Evaporation Heat Transfer and Pressure Drop of Refrigerant R-410A Flow in a Vertical Plate. *Journal of Heat Transfer-Transactions of the Asme*, 125(5):852–857, 2003. doi: 10.1115/1.1518498.
- [27] Giovanni A. Longo, Simone Mancin, Giulia Righetti, and Claudio Zilio. A new model for refrigerant boiling inside Brazed Plate Heat Exchangers (BPHEs). *International Journal of Heat and Mass Transfer*, 91:144–149, 2015. ISSN 00179310. doi: 10.1016/j.ijheatmasstransfer.2015.07.078.
- [28] Y Yan, HC Lio, and T Lin. Condensation heat transfer and pressure drop of refrigerant R-134a in a plate heat exchanger. *International Journal of Heat and Mass Transfer* 31, 121:936–1006, 1999. doi: 10.1016/S0017-9310(98)00217-8.
- [29] Bernard Thonon and A. Bontemps. Condensation of pure and mixture of hydrocarbons in a compact heat exchanger: Experiments and modelling. *Heat Transfer Engineering*, 23(6):3–17, 2002. ISSN 01457632. doi: 10.1080/01457630290098718.
- [30] D.H. Han, K.Y. Lee, and Y.H. Kim. The characteristics of condensation in brazed plate heat exchangers with different chevron angles. *Journal of the Korean Physical Society*, 43(1):66–73, 2003. ISSN 13594311. doi: 10.1016/S1359-4311(03)00061-9.
- [31] Giovanni A. Longo, Giulia Righetti, and Claudio Zilio. A new computational procedure for refrigerant condensation inside herringbone-type Brazed Plate Heat Exchangers. *International Journal of Heat and Mass Transfer*, 82:530–536, 2015. ISSN 00179310. doi: 10.1016/j.ijheatmasstransfer.2014.11.032.
- [32] Ji Zhang, Martin Ryhl Kærn, Torben Ommen, Brian Elmegaard, and Fredrik Haglind. Condensation heat transfer and pressure drop characteristics of R134a, R1234ze(E), R245fa and R1233zd(E) in a plate heat exchanger. *International Journal of Heat and Mass Transfer*, 128:136–149, 2019. ISSN 00179310. doi: 10.1016/j.ijheatmasstransfer.2018.08.124.

Bibliography

- [33] K Stephan and M. Korner. Berechnung des warmeubergangs verdamfender binarer flussigkeitsgemische. *Chem. Ing. Tech.*, 41(7):409–417, 1969. doi: 10.1002/cite.330410702.
- [34] H Jungnickel, P Wassilew, and W E Kraus. Investigations on the heat transfer of boiling binary refrigerant mixtures. *International Journal of Refrigeration*, 3(3):129–133., 1980. ISSN 0140-7007. doi: [https://doi.org/10.1016/0140-7007\(80\)90092-4](https://doi.org/10.1016/0140-7007(80)90092-4).
- [35] E.U. Schlunder. Heat transfer in nucleate boiling of mixtures. *Int. Chem. Eng.*, 23(4):589–599, 1983.
- [36] John R. Thome and S. Shakir. A new correlation for nucleate pool boiling of aqueous mixtures. *AICHE Symposium Series*, 83(257):46–51, 1987.
- [37] Yasunobu Fujita and Masayuki Tsutsui. Heat transfer in nucleate pool boiling of binary mixtures. *International Journal of Heat and Mass Transfer*, 37(1):291–302, 1994. ISSN 18792189 and 00179310. doi: 10.1016/0017-9310(94)90030-2.
- [38] Yasunobu Fujita and Masayuki Tsutsui. Heat transfer in nucleate boiling of binary mixtures (development of a heat transfer correlation). *JSME International Journal Series B Fluids and Thermal Engineering*, 40(1):134–141, 1997. ISSN 09168451. doi: 10.1299/jsmеб.40.134.
- [39] T Inoue, S Kawae, and M Monde. Characteristics of heat transfer during nucleate pool boiling of binary mixtures. *Heat and Mass Transfer*, 33(4):337–344, 1998. doi: <https://doi-org.proxy.findit.dtu.dk/10.1007/s002310050199>.
- [40] E Gungor and R H S Winterton. A general correlation for flow and annuli boiling in tubes. *International Journal of Heat and Mass transfer*, 29(3):351–358, 1986.
- [41] E Gungor and R H S Winterton. Simplified general correlation for saturated flow boiling and comparisons of correlations with data. *Chemical Engineering Research and Design*, 65(2):148–156, 1987.
- [42] D.S. Jung, M. McLinden, R. Radermacher, and D. Didion. A study of flow boiling heat transfer with refrigerant mixtures. *International Journal of Heat and Mass Transfer*, 32(9):1751–1764, 1989. ISSN 00179310. doi: 10.1016/0017-9310(89)90057-4.
- [43] Matthias Wettermann and Dieter Steiner. Flow boiling heat transfer characteristics of wide-boiling mixtures. *International Journal of Thermal Sciences*, 39(2):225–235, 2000. ISSN 12900729. doi: 10.1016/S1290-0729(00)00241-6. URL <http://linkinghub.elsevier.com/retrieve/pii/S1290072900002416>.
- [44] Farzad Vakili-Farahani, Raffaele L Amalfi, and John R Thome. Two-Phase Heat Transfer and Pressure Drop within Plate Heat Exchangers. In John R. Thome and Jungho Kim, editors, *Encyclopedia of Two-Phase Heat Transfer and Flow II : Special topics and applications. Volume 2: Boiling Using Enhanced Surfaces*,

Bibliography

- Plate Heat Exchangers and Two-Phase Devices*, chapter 4, pages 145–215. World Scientific Publishing, 2015. ISBN 978-981-4623-29-2. doi: https://doi.org/10.1142/9789814623285_0011.
- [45] R.W. Lockhart and R.C. Martinelli. Proposed correlation of data for isothermal two-phase, two-component flow in pipes. *Chemical engineering progress*, 45(1):39–48, 1949.
 - [46] D Chisholm. A Theoretical Basis for the Lockhart-Martinelli Correlation for Two-Phase Flow. *International Journal of Heat and Mass Transfer*, 10(18):1767–1778, 1967. ISSN 00179310. doi: [http://dx.doi.org/10.1016/0017-9310\(67\)90047-6](http://dx.doi.org/10.1016/0017-9310(67)90047-6). URL <http://www.sciencedirect.com/science/article/pii/0017931067900476>.
 - [47] Giovanni Longo and Andrea Gasparella. Refrigerant R134a vaporisation heat transfer and pressure drop inside a small brazed plate heat exchanger. *International Journal of Refrigeration*, 30:821–830, 2007. doi: <10.1016/j.ijrefrig.2006.11.011>.
 - [48] Y. Y. Hsieh and T. F. Lin. Saturated flow boiling heat transfer and pressure drop of refrigerant R-410A in a vertical plate heat exchanger. *International Journal of Heat and Mass Transfer*, 45(5):1033–1044, 2002. ISSN 00179310. doi: [10.1016/S0017-9310\(01\)00219-8](10.1016/S0017-9310(01)00219-8).
 - [49] John R Thome and Andrea Cioncolini. Void fraction. In John R Thome, editor, *Encyclopedia of Two-Phase Heat Transfer and Flow I, Volume 3: Flow boiling in Macro and Microchannels*, chapter 4, pages 85–112. . doi: 10.1142/9789814623216_0021. URL https://www.worldscientific.com/doi/abs/10.1142/9789814623216_0021.
 - [50] S.M. Zivi. Estimation of Steady-State Steam Void-Fraction by Means of the Principle of Minimum Entropy Production. *Journal of Heat Transfer - Transactions of the ASME*, 86(2):247–252, 1964. doi: <10.1115/1.3687113>.
 - [51] S. L. Smith. Void fractions in two-phase flow: a correlation based upon an equal velocity head model. *Proceedings of the Institution of Mechanical Engineers*, 184(1): 647–664, 1969. ISSN 0020-3483. doi: 10.1243/PIME_PROC_1969_184_051_02.
 - [52] S.Z. Rouhani and E. Axelsson. Calculation of void volume fraction in the subcooled and quality boiling regions. *International Journal of Heat and Mass Transfer*, 13(2): 383–393, 1969. ISSN 18792189. doi: [10.1016/0017-9310\(70\)90114-6](10.1016/0017-9310(70)90114-6).
 - [53] John R Thome and Andrea Cioncolini. Two-phase pressure drop. In John R Thome, editor, *Encyclopedia of Two-Phase Heat Transfer and Flow I*, chapter 6, pages 143–176. . doi: 10.1142/9789814623216_0023. URL https://www.worldscientific.com/doi/abs/10.1142/9789814623216_0023.
 - [54] SWEP International AB. SWEP Products, 2015. URL <https://www.swep.net/products/>.

Bibliography

- [55] Eric Granryd, Ingvar Ekroth, Per Lundqvist, Åke Melinder, Björn Palm, and Peter Rohlin. *Refrigerating engineering*. Royal Institute of Technology, KTH, Department of Energy Technology, Division of Applied Thermodynamics and Refrigeration, 2009. ISBN 9789174154153.
- [56] Benjamin Zühlsdorf, Jonas Kjær Jensen, and B. Elmegaard. Heat pump working fluid selection – economic and thermodynamic comparison of criteria and boundary conditions. *International Journal of Refrigeration*, 2018. ISSN 0140-7007. doi: <https://doi.org/10.1016/j.ijrefrig.2018.11.034>. URL <http://www.sciencedirect.com/science/article/pii/S0140700718304870>.
- [57] Sivert Vist and Jostein Pettersen. Two-phase flow distribution in compact heat exchanger manifolds. *Experimental Thermal and Fluid Science*, 28:209–215, 2004. ISSN 08941777. doi: 10.1016/S0894-1777(03)00041-4.
- [58] Shenghan Jin and Pega Hrnjak. Effect of end plates on heat transfer of plate heat exchanger. *International Journal of Heat and Mass Transfer*, 108:740–748, 2017. ISSN 00179310. doi: 10.1016/j.ijheatmasstransfer.2016.11.106. URL <http://dx.doi.org/10.1016/j.ijheatmasstransfer.2016.11.106>.
- [59] Wenzhe Li and Pega Hrnjak. An experimentally validated model of single-phase flow distribution in brazed plate heat exchanger. In *17th International Refrigeration and Air Conditioning Conference at Purdue*, 2018.
- [60] H Versteeg and W Malalasekera. *An introduction to computational fluid dynamics: the finite volume methods*. Longman scientific and technical, 1995. ISBN 0582218845 and 0470235152.
- [61] E.W. Lemmon, M.L. Huber, and M.O. McLinden. NIST Standard Reference Database 23, 2013. URL <http://www.nist.gov/srd/upload/REFPROP9.pdf>.
- [62] Ian H. Bell, Jorrit Wronski, Sylvain Quoilin, and Vincent Lemort. Pure and pseudo-pure fluid thermophysical property evaluation and the open-source thermophysical property library coolprop. *Industrial and Engineering Chemistry Research*, 53(6): 2498–2508, 2014. ISSN 08885885. doi: 10.1021/ie4033999.
- [63] Python Software Foundation. Python 3.7.1 documentation, 2018. URL <https://docs.python.org/release/3.7.1/>.
- [64] Ian H. Bell and the CoolProp team. Low level interface, 2018. URL <http://www.coolprop.org/coolprop/LowLevelAPI.html>.